IDENTIFICATION OF NOVEL SMALL MOLECULE INHIBITORS OF YAP-TEAD BINDING WITHIN THE HIPPO SIGNALING PATHWAY

Abigail Fisk Thompson

Submitted to the faculty of the University Graduate School
in partial fulfillment of the requirements
for the degree
Master of Science
in the Department of Biochemistry and Molecular Biology,
Indiana University

September 2020

Accepted by the Graduate Faculty of Indiana University, in partial fulfillment of the requirements for the degree of Master of Science.

Master's Thesis Committee

Clark D. Wells, PhD, Chair

Millie M. Georgiadis, PhD

Mark G. Goebl, PhD

Steven M. Johnson, PhD

ACKNOWLEDGEMENT

First and foremost, I would like to thank Dr. Clark Wells for mentoring me and taking me in as a graduate student with no prior research experience. He has always been patient with me, taught me many laboratory skills, and gave me a wonderful educational experience. I would also like to thank my committee members for their guidance and flexibility throughout the year, especially during the COVID-19 pandemic when labs were shut down. Thank you to Kevin Lange for being a great lab mate and showing me the way around lab. Lastly, I would like to thank my parents, Angie and Jerry Thompson, and my boyfriend Quinn for their constant support through my year as a graduate student and always encouraging me to chase my dreams.

Abigail Fisk Thompson

IDENTIFICATION OF NOVEL SMALL MOLECULE INHIBITORS OF YAP-TEAD BINDING WITHIN THE HIPPO SIGNALING PATHWAY

The Hippo signaling pathway controls organ size by regulating cell proliferation, apoptosis, and cell differentiation. The Hippo pathway ultimately regulates the concentration of the coactivator yes-associated protein 1 (YAP1) in the nucleus, which binds the transcription factor TEA domains (TEAD), activating genes related to cell proliferation. In several cancers, increased YAP1 activity is linked to increased cellular proliferation, de-differentiation and survival to drive tumor progression and spreading. The development of inhibitors against YAP-TEAD binding are consequently a research topic of much interest. While several inhibitors of the YAP-TEAD interaction are reported, none possess both high specificity and anti-tumor activity. The work described here is based upon a collaboration with AtomWise, Inc to find a best in class competitive inhibitor of YAP-TEAD binding. AtomWise completed a computational screen of ten million compounds for potential binding to a TEAD pocket that is essential for interaction with YAP1. This master's thesis encompasses both intracellular and biochemical validation of these compounds. Initially, a luciferase YAP/TEAD dependent reporter assay was used to identify compounds with potential intracellular activity. This data was compared with the action of these compounds on the metabolic activity (MTT assay) across three cancer cell lines. Three sulfonamide-based compounds, **4**, **22**, and **59** were identified as top 10 YAP/TEAD inhibitors. Six additional compounds were synthesized that combined specific moieties in these three compounds. Dose response

curves for inhibition of TEAD reporter activity showed that compounds **22** and **59** exhibited both high inhibition and low IC_{50} values relative to the derivatives. Further, compound **22** also significantly reduced the levels of *CTGF* transcript (measured by RT-qPCR), a surrogate measure for endogenous YAP1: TEAD activity. Preliminary fluorescent polarization data also suggests that compound **22** inhibits the binding of a 5(6)-FAM labeled YAP1 peptide (residues 58-74) to a purified TEAD fragment.

In this work, compounds **22** and **59** are found to inhibit TEAD dependent transcription and the growth of multiple cancer cell lines. In addition, promising preliminary biochemical data indicates that compound **22** may inhibit the interaction of YAP1 with TEAD.

Clark D. Wells, PhD, Chair

TABLE OF CONTENTS

LIST OF TABLES

LIST OF FIGURES

LIST OF ABBREVIATIONS

ADME	Absorption, distribution, metabolism, and excretion
ADPKD	Autosomal dominant polycystic kidney disease
cDNA	Complimentary deoxyribonucleic acid
DNA	Deoxyribonucleic acid
CTGF	Connective tissue growth factor
DMEM	Dulbecco's Modified Eagle Medium
DMSO	Dimethyl sulfoxide
ECM	Extracellular matrix
EGFR	Epidermal growth factor
LATS1/2	Large tumor suppressor 1/2 kinase
mRNA	Messenger ribonucleic acid
Mst1/2	Mammalian STE20-like protein kinase
NADPH	Nicotinamide adenine dinucleotide phosphate
PBS	Phosphate buffered saline
PCR	Polymerase chain reaction
PEI	Polyethyleneimine
PKD	Polycystic kidney disease
QToF MS	Quadruple-time of flight mass spectroscopy
rRNA	ribosomal ribonucleic acid
RT-qPCR	Real time quantitative polymerase chain reaction
SAR	Structure-activity relationship
SAV1	Salvador homolog 1

SDS-PAGE	Sodium-dodecyl sulfate polyacrylamide gel electrophoresis
TAZ	Transcription co-activator with PDZ -binding motif
TEAD1-4	TEA domain
TK Renilla	Thymidine Kinase Renilla
YAP1	YES-associated protein 1

CHAPTER 1: INTRODUCTION

1.1 The Hippo Pathway

The Hippo pathway promotes cell differentiation and apoptosis while inhibiting cell movement and growth to influence organ size and to suppress tumor formation [1]. Anti-growth cues including cell stresses and cell-cell contacts activate HIPPO signaling [2]. Whereas, cell-extracellular matrix interactions and growth factor signaling inhibit the HIPPO pathway [3]. Core HIPPO signaling involves the activation of the large tumor suppressor (LATS) kinases via phosphorylation by the Mst1/2 kinases that occurs in response to upstream signals including cell-cell contacts and cell polarity [3]. Active LATS1/2 then phosphorylate and functionally suppress the ability of YES-associated protein 1 (YAP1) to activate transcription factors [4]. Phosphorylation inhibits YAP1 by targeting it for 14-3-3 mediated sequestration in the cytoplasm and for proteasomal degradation [5]. Conversely, accumulation of non-phosphorylated YAP1 in a background of low HIPPO signaling results in high levels of nuclear YAP1 that co-activates TEA domain (TEAD1-4) and other transcription factors [6]. Consequently, genes associated with cell proliferation and cell survival are actively transcribed (**Figure 1**) [7].

Cell contacts and mechanical loading play oppositional roles in the regulation of the Hippo pathway [8-10]. Cells in tissues interact with their neighbors to form differentiated structures [11]. The resultant intercellular contacts promote high intracellular HIPPO signaling that prevents the accumulation of YAP1 in the nucleus [12]. Conversely, when cells have sparse contacts with other cells, the cytosolic levels of YAP1 increase [12]. In parallel, mechanical loading on the cell by a threshold of extracellular matrix (ECM) stiffness stimulates YAP1 to be imported into the nucleus [5].

These findings were mainly uncovered by experiments studying cells growing in matrices of varying stiffness usually by altering the composition of collagen in Matrigel [13]. Additionally, YAP1 was shown to accumulate in the cytoplasm but not enter the nucleus in cells that are detached from their underlying substratum [14].

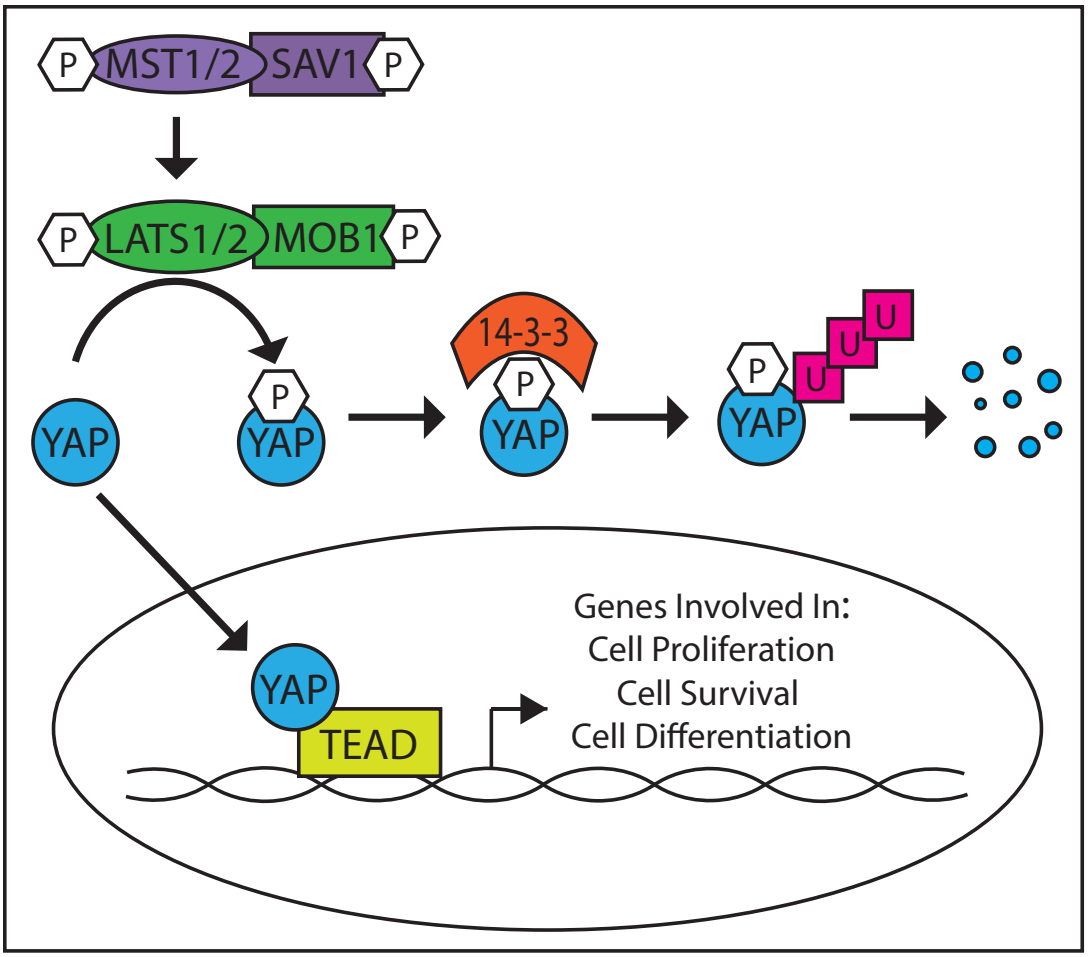

Figure 1. Schematic representation of the Hippo Signaling Pathway. When phosphorylated by LATS Kinases, YAP1 is sequestered in the cytoplasm and is eventually degraded by ubiquitin mediated proteasomal degradation. YAP1 can enter the nucleus and bind TEAD when not phosphorylated, activating genes involved in cell proliferation, survival, and differentiation.

1.2 Two examples of YAP1 and human disease

The initiation and progression of many cancers are highly dependent on the activation of YAP1, meaning the Hippo pathway is inactive and YAP1 is unphosphorylated and enters the nucleus. [15]. In multiple types of solid tumors, YAP1 levels and activity are upregulated in the tumor tissue relative to adjacent normal tissue [16]. A meta-analysis of 21 studies totaling 2983 patients found that the overexpression of YAP1 is associated with poor prognosis and reduced rates of survival across several types of cancer [17]. This is due to the amplification of the YAP1 gene in cancers of the lung, pancreas, esophagus, liver, and breast [18]. Whereas, increased transcript levels of YAP1 in the absence of gene amplification are observed in many other types of human cancer [19]. Because TEADs have been found to be essential for the pro-cancer effects of YAP1, the development of molecules that inhibit YAP1 binding to TEADs is an active area of anti-cancer research [20].

In addition to cancer, several other diseases including autosomal dominant polycystic kidney disease (ADPKD) are associated with aberrant YAP1 activity [21]. ADPKD is the fourth leading cause for kidney transplants and kidney related deaths [22]. ADPKD is characterized by the spontaneous formation of fluid filled cysts in about 1 % of renal tubules [23]. The continuous enlargement of these cysts eventually leads to renal failure [24]. While mutational inactivation of *Pkd1* or *Pkd2,* which code for polycystin proteins that play roles in cell-cell signaling, accounts for 85 % of ADPKD cases [25, 26], a gene set enrichment analysis showed an enrichment of TEAD target genes, including *c-Myc,* in human polycystic kidney samples [27]. Further work showed that

Pkd1 inactivation results in YAP1 dephosphorylation and nuclear accumulation [28]. YAP1 activation is therefore proposed to drive cyst growth following *Pkd1* deficiency [27]. Currently, kidney transplant is the only treatment for PKD [29]. A small molecular inhibitor of YAP1-TEAD binding could therefore delay the damage caused by cyst growth to increase the window for transplant before renal failure.

1.3 YAP-TEAD binding interface

Multiple crystal structures of fragments of YAP1 bound to different TEAD1, TEAD2, and TEAD4 to reveal three conserved binding interfaces (**Figure 2**) [30, 31]. The consensus minimal TEAD-binding region in YAP1 comprises three sequential elements. The first region (residues 50-56) consists of an anti-parallel beta-sheet that interacts with TEAD through main chain hydrogen bonding [30]. Consistent with reports that these bonds contribute minimally to overall binding, deletion of residues 50-56 in YAP1 results in minimal differences in its binding affinity for TEAD [32]. Taken together, the lack of specificity of the beta sheet interface and its small energetic contribution to binding argues against targeting this interface to inhibit YAP1 binding to TEAD. The second region (residues 61-73) forms an alpha-helix that binds to a hydrophobic pocket in TEAD [30]. Three residues, Leu65, Leu68, and Phe69, lie along the alpha-helical interface that contacts TEAD to form an LxxLF motif, which is known to bind to hydrophobic grooves [33]. Further, Phe69 directly contacts residues within the TEAD hydrophobic pocket and serves as the rotation center for YAP1 (**Figure 3**)[34]. The important contribution of Phe69 for binding was affirmed by experiments showing that substitution with Ala increases the K_d from 18 nM in wild type YAP1 to 6447 nM

[35]. The identification of molecules that bind to the pocket in TEAD that binds Phe69 is therefore a highly attractive strategy to inhibit YAP1-TEAD binding. Region three (residues 85-99) comprises a twisted coil region referred to as an omega loop [30]. Hydrophobic side chains on residues M86, L91, and F95 in the YAP1 omega loop form van der Waals interactions with several hydrophobic residues within a pocket on TEAD that is formed by three beta strands and two alpha helices (Beta 4, 11, and 12 and alpha 1 and 4)[36]. This interface is further strengthened by an interaction between R89 of YAP1 and the carboxylate oxygen of an aspartate in TEAD [36]. Studies have shown that the omega loop interface is necessary for the efficient binding of YAP1 and TEAD [32] and multiple groups have targeted this interface for drug discovery. The YAP1 binding domain has shown to have 100% identity among the four TEADs, meaning one inhibitor of the alpha-helical region should work for all TEADs [38].

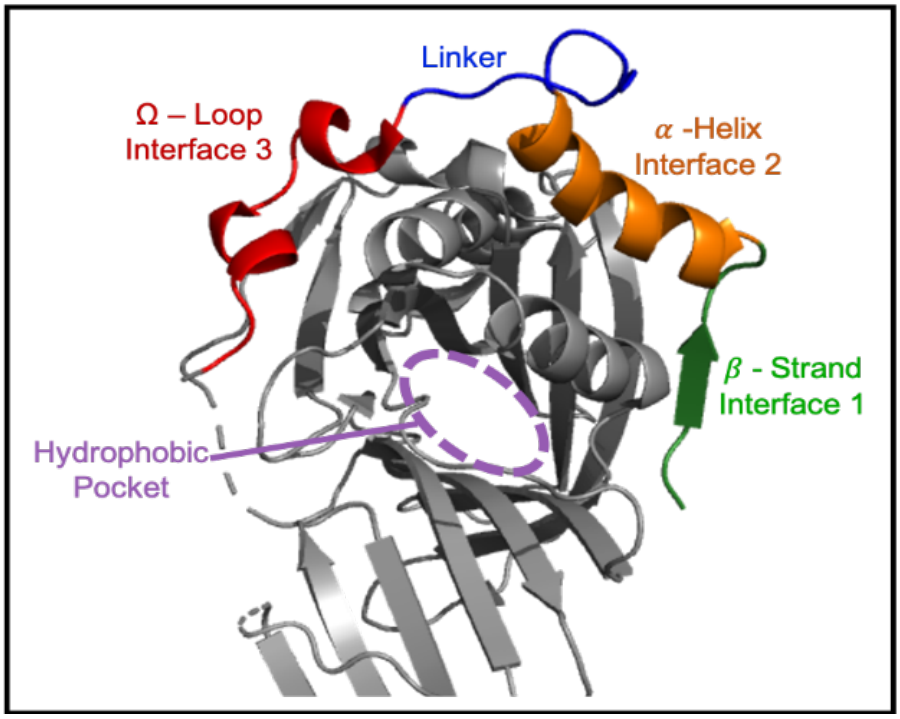

Figure 2. Illustration of the YAP1-TEAD1 binding interfaces. TEAD2 is shown in grey bound to the YAP1$^{52-56}$ beta strand, YAP1$^{61-73}$ alpha helix, and YAP1$^{85-99}$ omega loop. (PDB: 3KYS)

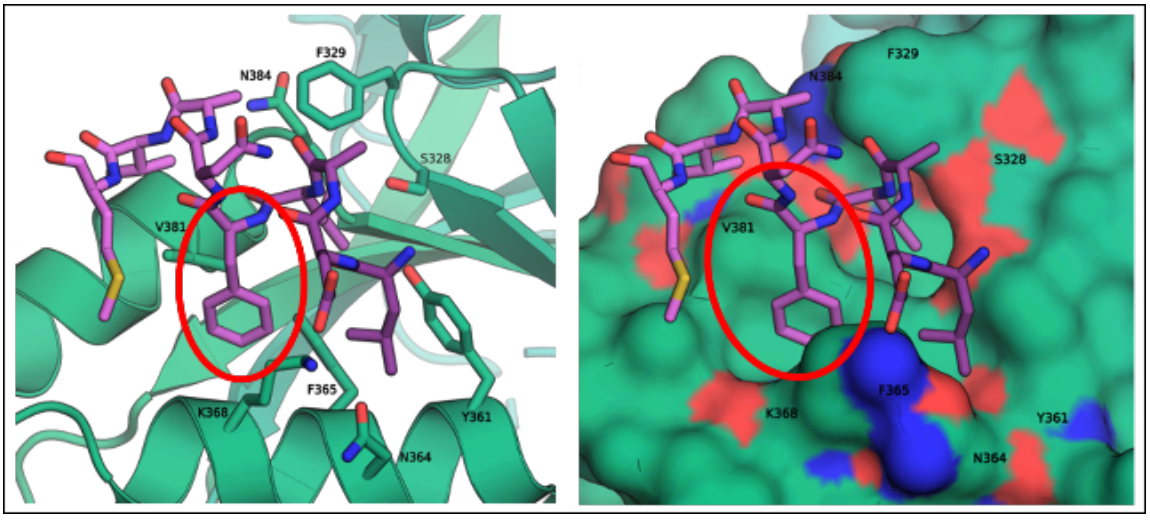

Figure 3. Structural representations of YAP1 alpha-helical region interaction with TEAD2. Phe69 within the alpha-helical interface 2 of the YAP1-TEAD binding surface fits into a binding pocket on TEAD2 (depicted in left panel as a ribbon plot and in right panel as a surface density plot, both plots were prepared by Neil Henrikson at AtomWise Inc.). PDB: 3KYS

1.4 Palmitoylation of TEAD

The post-translational palmitoylation of a conserved cysteine in all TEAD members promotes their stability and potentially binding to YAP1 [37]. While the consensus of numerous studies is that a cysteine residue buried in a hydrophobic pocket in TEAD is efficiently autopalmitoylated, the effects of this modification are controversial. Although initial reports found that palmitoylation of TEAD is essential for binding to YAP1, more recent studies find that mutants that lack the autopalmitoylated cysteine are highly unstable [38]. Further, a cysteine to alanine TEAD mutant showed a complete loss of stable protein in cells [39]. Conversely, another study found that the palmitoylation of TEAD plays no role in its localization, but is required for binding to YAP1 [37]. In either case, the key role that palmitoylation plays in the stability of TEAD and potentially its binding to YAP1 necessitates its consideration as part of an effort to develop inhibitors against YAP1-TEAD binding. This has been directly addressed by several reports showing that small molecules that covalently bind to the conserved cysteine in TEAD inhibit the interaction of TEAD with YAP1. However, no studies have examined how palmitoylation of TEAD may impact competitive inhibitors of YAP1-TEAD, which may explain why compounds with promising inhibitory effects in vitro have failed to have strong effects in vivo.

1.5 Overview of previous efforts to develop inhibitors of YAP1-TEAD binding

Peptides based on the YAP1 sequence have shown promise as competitive inhibitors of YAP1-TEAD binding. Therapeutic peptides are straightforward to synthesize and generally show high specificity for binding their target with low toxicity.

A peptide containing the sequence of the flexible omega-loop in YAP1 can inhibit YAP1 binding to TEAD with an IC_{50} of 37.0 μM [40]. Peptides with amino acid substitutions that decrease the flexibility of the omega-loop peptide and consequently increase the binding to TEAD, including the introduction of cysteines to cyclize the peptide via a disulfide bond [40], can achieve an IC_{50} of as low as 1.81 uM for preventing YAP1 binding to TEAD[40]. However, it is unclear whether this peptide avoids common issues associated with other peptides such as metabolic instability, poor oral bioavailability, low cellular uptake, and rapid clearance [41].

Small molecule approaches have also shown some promise for competitively inhibiting the binding of YAP1 to TEAD. However, no reported compounds have shown both specific anti-YAP1-TEAD activity and strong anti-tumor effects. Initially, the FDA approved drug verteporfin was pursued as a promising YAP1-TEAD inhibitor. Verteporfin is used in the clinic as a laser activated drug to remove blood vessels growing underneath the retina in macular degeneration [42]. Pan and colleagues subsequently identified Verteporfin as an inhibitor of YAP1-TEAD in a luciferase reporter assay. Importantly, they found that Verteporfin treatment also prevented YAP1-induced liver overgrowth in mice [20]. Consequent studies found that Verteporfin inhibits the growth of several breast cancer lines and that it is particularly effective at blocking the growth of breast cancer cells lines with high YAP1 expression. However, the relatively high concentrations of verteporfin that were needed to inhibit growth (1 -10 μM) did not correlate with the levels of YAP1 expression across the cell lines tested [43]. Similar results were found for bladder, gastric, and ovarian cancer cell lines [44-46]. In addition, even though verteporfin was reported 8-years ago to inhibit YAP1-TEAD, there is still no

structural information on how verteporfin interacts with this complex. Further, verteporfin has been found to exert antitumor properties through several non-HIPPO pathway targets. For instance, verteporfin inhibits the growth of endometrial cancers via its interaction with epidermal growth factor receptor (EGFR) in a YAP1-independent manner [47]. Verteporfin also binds to p62 to inhibit autophagy, which results in a loss of cell growth [48]. Verteporfin therefore appears to have a broad range of targets whose inhibition may result in reducing cancer cell growth that are independent of YAP1-TEAD. These issues are compounded with other chemical limitations of verteporfin including its difficulty to synthesize, limited solubility and light sensitive stability.

As previously mentioned, several groups have developed covalent inhibitors directed against the cysteine in TEADs that is palmitoylated. The hydrophobic pocket containing the palmitoylated cysteine residue is thought to stabilize TEAD and improve its ability to bind to YAP1 [39]. Consistently, small molecules that covalently bind this cysteine have shown potent inhibition of bacterially expressed TEADs binding to YAP1 [49]. However, these compounds generally have an electrophile that can covalently modify the reactive cysteine trough that is buried in the hydrophobic pocket of TEADs, preventing the palmitoylation of TEADs. These compounds may therefore have significant activity to surface exposed cysteines of other proteins that they come into contact. Further, it is unclear whether palmitate has a high off rate from TEADs in cells and whether the compounds can effectively displace palmitate from a majority of intracellular TEADs.

Recently, celastrol was reported to prevent YAP1-TEAD binding. Celastrol is isolated from the roots of the plant *Celastrus regelii* and has anti-obesity effects in mice.

In 2015, celastrol was reported to curb food intake by nearly 80 percent causing up to 45 percent weight loss in mice tested [50] by potentially sensitizing the hunger modulating effects of the lepton hormone to the brain [51]. More recently, celastrol was shown to significantly reduce YAP1 transcriptional targets including *CTGF* by 65 percent. Celastrol also reduced the rate of proliferation and viability of H1299 lung and MDA-MB-231 breast cancer cell lines [52]. However, when the concentration of Celastrol was reduced from 5 μM to 1 μM, *CTGF* levels were only reduced by 10 percent. While the anti-cancer effects of Celastrol are promising, there is no direct evidence that celastrol binds to TEADs.

1.6 Current work on compounds predicted by AtomWise, Inc to bind the Ph69 binding pocket in TEAD

AtomWise, Inc uses artificial intelligence to enhance drug discovery. AtomWise developed AtomNet, an algorithm that uses a deep convolutional neural network to improve structure-based drug discovery. Convolution neural networks break down complex concepts into smaller fragments of information that are analyzed in isolation and then pieced back together [54]. Convolution neural networks have had recent success in image classification, speech recognition and face recognition [54]. For example, convolution neural networks recognize a face by first "learning" the features of the edge of the face and then by putting these edges back together to establish similarities between larger parts of the face, including eyes, ears, and noses [54]. The system then learns how to combine the individual face parts to gain a high certainty for recognition of a whole face. AtomNet used this method to "learn" the trends and rules within organic chemistry

that were then combined to recognize important chemical groups that dictate interactions between ligand and protein interfaces [54]. AtomWise has been contracted for drug discovery with companies including Merck, Eli Lilly, Bayer, Abbvie, and for many educational research institutions though the Artificial Intelligence Molecular Screen (AIMS) award program. This program accepts grant applications from academic research institutions across the world that are interested in finding a small molecule that binds a specific target. Over 300 AIMS awards have been granted to a broad range of projects involving animal health, biotechnology, human biology, medicine, microbiology, plant biology, and virology. The targets of AIMS awardees are subject to a customized small molecule virtual screen using AtomNet technology, which screens over ten million compounds for binding abilities. The researcher then receives around 70 small molecules that are predicted to bind to the target.

Dr. Wells and Dr. Georgiadis were awarded an AtomWise, Inc AIMS grant to computationally screen 10 million compounds for their likelihood to bind to the hydrophobic pocket of TEAD1 that binds Phe69 in YAP1. AtomWise employed their unique AI-directed docking algorithms to predict molecules that should bind TEAD in a pocket that binds Phe69 within the alpha-helical region of YAP1. From this screen, 76 “hit” compounds were delivered. My master’s thesis carried out an intracellular and biochemical validation of these 76 small molecules for their ability to inhibit the binding and activation of TEADs by YAP1.

CHAPTER 2: METHODS

2.1 Silencing of YAP1 in HeLa Cells

Following trypsinization, HEK-293T cells were plated and grown to 70% confluency in 10 cm plates. Media was then aspirated and replaced with 8 mL of serum free DMEM containing the PEI transfection mixture. This transfection mixture was created by mixing 50 µg PEI dropwise (25 µl) into 1 mL serum free DMEM that contains 6 µg pVSV, 5 µg pRSV-REV, 10 µg pRRE, and 20 µg shYAP. Cells were incubated with the transfection mixture at 37° C and 5% CO_2 for 16 hours. The media was then replaced with 7 mLs complete DMEM (10% fetal bovine serum) containing 10 mM HEPES pH 7.5. The cells were incubated for an additional 18 h at 37° C in 5 % CO_2 before the media containing virus was collected. After any cellular material was removed from the media by centrifugation, 27 µL of 5 mg/mL of polybrene was added per 7 mLs of media with virus. Viral media with polybrene was then diluted 1:3 with complete DMEM. After removing the media from a 10 cm plate with 30 % confluent HeLa cells, 3 mL of diluted virus was added. After 24 hours, virus containing media was aspirated and replaced with complete DMEM. At 24 hours after infection cells were split for assays and for measuring YAP1 silencing by immunoblot analysis. At 48 hours of viral infection, 60 cm dishes of cells were harvested in 100 µL of lysis buffer (100 mM Tris pH 8.5, 10 mM urea, 2 mM sodium orthovanadate, and 25 mM beta-glycerol phosphate). Protein lysates were then analyzed by immunoblot for relative levels of YAP1 and beta-tubulin. Additionally, cells were reverse transfected into 24-well plates 24 hours post infection with the TEAD reporter and Renilla reporter constructs. After 48 hours, these cells were harvested in passive lysis buffer. The firefly/Renilla luciferase activity in 20 µl

of lysate from each well was measured using the Duo Luciferase Genecopoeia kit (cat # LF001).

shYAP1 Construct – V3875: GCCACCAAGCTAGATAAAGAA
shScramble Construct – V3325: CCTAAGGTTAAGTCGCCCTCGCTCTAG CGAGGGCGACTTAACCTTAGG

2.2 Immunoblot Analysis

Cells were washed with ice cold PBS and then detached in 1mL PBS with a rubber spatula. Cells were transferred to a 1.5 mL micro centrifuge tube and collected by centrifugation at 5000 RPM for 5 minutes using an Eppendorf 5424. Cell pellets were lysed for 5 min on ice with 100 µL of lysis buffer (50 µL 1M Tris buffer pH 8.5, 0.24 g Urea, 10 µL 100x ProteCEASE™ protease inhibitor, 10 µL 100x sodium orthovanadate, 100 µL 10x beta glycerol phosphate). Post nuclear supernatants were clarified by centrifugation at 10,000 RPM at 4° C for 5 minutes. Clarified lysates were collected and stored at -80 °C or subjected to sodium-dodecyl sulfate-polyacrylamide gel electrophoresis (SDS-PAGE). For SDS-PAGE, 20 µL of lysate was added to 4µl of 6X sample buffer. Samples were then denatured at 95° C for 5 minutes. Protein samples were then loaded using a Hamilton syringe into individual wells of a 12 % SDS polyacrylamide gel. Protein were resolved through gel at 150V for 90 minutes. Proteins were then transferred from a gel to a nitrocellulose membrane at 12V for 90 minutes using a GENIE electrophoretic transfer system in transfer buffer (25 mM Tris pH 7.6, 192 mM glycine, 20 % methanol, and 0.03% SDS). After transfer, membranes were blocked with 5% powdered milk in tris-buffered saline. Blots were then washed 3X with Tris-buffered saline with 0.05% Tween-20 (TBST) for five minutes with rocking at room temperature. The membrane was then transferred into a hybridization bag and 3 mLs of

TBST, 1µl of a mouse anti-Beta tubulin antibody (1:3000) and 3 µl of rabbit anti-YAP1 antibody (1:1000) was added before the bag was sealed. The membrane was then incubated with the antibodies at 4° C with rocking on a nutator for 2 hours. The corner of the bag was then cut and the antibody mix was recovered for re-use of up to 3 times. The membrane was then removed from the bag and transferred to a grey plastic box for washing with TBST three times for 5 minutes at room temperate on a rotary shaker. After removal of the last wash, 10 mLs of TBST were then added which contained a goat anti-mouse secondary antibody diluted 1:20,000 and a Donkey anti-Rabbit antibody diluted 1:20,000. The box containing the membrane and antibodies was then covered by a second stackable box and it was returned to the rotary shaker for 30 minutes with rocking at room temperature. After washing the membrane for 3X in TBST for 5 minutes, the nitrocellulose membrane was imaged using a LiCor © Odyssey machine.

2.3 Luciferase Reporter Assay in HeLa Cells

The day before an assay, HeLa cells were split 1:2 so that cells would be in log phase growth. The following day, cells were reverse transfected with the reporter construct. For each transfection, the pGL3.1 plasmid containing the CTGF promoter (0.13 µg/well) and the TK Renilla (0.13 µg/well) plasmid were added to 500 µL of serum free DMEM. PEI (2 µg/well) was added to DNA mixture with vortexing and was incubated at room temperature 10 minutes. The mixture was added to non-adherent HeLa cells at a density of 40,000 cells per well and serum free DMEM to reach a final volume of 500 µL per well. The cell mixture was plated in 24 well plates and left in tissue culture hood to settle for 20 minutes. Cells were then incubated at 37° C and 5 % CO_2 for two hours. The media was aspirated off cells and replaced with compound dissolved in

DMSO diluted in DMEM/10 % fetal bovine serum. Cells were incubated with compound for 18 hours at 37° C and 5 % CO_2. Media was aspirated and cells were washed with 250 µL PBS on ice. Cells in each well were harvested with 100 µL of passive lysis buffer and rocked for 15 minutes. Lysates were transferred to 1.5 mL microcentrifuge tubes and spun down at 14,000 RPM at 4° C for 10 minutes. 20 µL of supernatant was transferred to new 1.5 mL microcentrifuge tubes and the firefly luciferase activity was measured in ratio with the control TK renilla luciferase activity, using the GeneCopoeia Luc-Pair™ Duo-Luciferase Assay Kit 2.0 (cat # LF001).

CTGF Luciferase Reporter Construct – V4088
TK Renilla Construct – V3605

2.4 MTT Assay

MIA, Pa14C, and H460 Cells were seeded at 10,000 cells per well in a 96 well plate in 55 µL of DMEM/10 % FBS supplemented with 3 % matrigel and incubated at 37° C and 5% CO_2. On day four, 55 uL of compounds at 40 µM were add to the cells and incubated for an additional four days. On day eight, 55 µL of 20 µM compound containing media was added. On day 12, 18 µL of 5 mg/mL MTT reagent in PBS was added to each well for 2 hours. 75 µL of the medium was removed and 100 µL of 16% SDS in 40% DMF with 2% glacial acetic acid was added to each well. The plate was incubated at 37° C and 5% CO_2 overnight and the absorbance was measured at 570 nm the following day.

Normal kidney cells, autosomal dominant polycystic kidney disease, and adjacent autosomal dominant polycystic kidney disease cells were seeded at 1,000 cells per well in a 96 well plate. Media was aspirated after 24 hours and replaced with 100 µL of media

containing compound. Cells were incubated with compound for 36 hours at 37° C and 5% CO_2. 20 µL of 5mg/mL MTT reagent in PBS was added to each well and returned to the incubator for 2 hours. After two hours, 100 µL of MTT solvent (4mM HCl and 0.1% Triton X in isopropanol) was added to each well. The plate was covered with foil and placed in the dark at room temperature for one hour. Absorbance of wells were measured at 570 nm after one hour.

2.5 Quantitative Real-Time Polymerase Chain Reaction (qRT-PCR)

HeLa cells were grown in DMEM with 10% FBS to 50% confluence in 6 cm plates and then treated with 20 µM compound for 24 hours. The cells were washed with 1 mL ice-cold PBS, harvested with 1 mL of Trizol, and incubated at room temperature for 5 minutes. 100 µL of chloroform was added and the samples were spun down for 10 minutes at 14,000 RPM at 4° C. The supernatant was transferred to new tubes and the RNA was precipitated out with 1 mL isopropanol. The sample was spun at 14,000 RPM for 10 minutes at 4° C and the supernatant was removed. The RNA was washed with 500 µL 70% ethanol, spun down, at 14,000 RPM for 5 minutes at 4° C, and the supernatant was removed. The RNA pellet was dried and was resuspended in 20 µL of H_2O. 5 µL of RNA was added to a mixture containing 10 µL H_2O, 2 µL oligo dT (50 µM), and 4 µL dNTPs (10 mM) and incubated for 5 minutes at 65° C. Complimentary deoxyribonucleic acid (cDNA) synthesis was completed by incubating the RNA, oligo dT and dNTP mixture with 10 µL H2O, 4 µL RT Buffer, and 2 µL SuperScript reverse transcriptase. The samples were incubated at 50° C for 45 minutes. The DNA concentration was measured using the NanoDrop© spectrophotometer and samples were diluted to 400

ng/μL with nuclease-free water. A mixture of 5 μL of the dilute cDNA, 10 μL of H_2O, 10 μL of SYBR Green PCR SensiMix (Bioline), and 1 μL of both forward and reverse primers were added to wells in a 96 well plate and assayed using the RealPlex ABI-FastOpti (Eppendorf) protocol. Values were normalized to 18S rRNA. Forward and reverse primers used are listed below.

18S rRNA Forward Primer:	CCGATAACGAACGAGACTCTGG
18S rRNA Reverse Primer:	TAGGGTAGGCACACGCTGAGCC
CTGF Forward Primer:	CCGTACTCCCAAAATCTCCA
CTGF Reverse Primer:	GTAATGGCAGGCACAGGTCT

2.6 TEAD2 Expression and Purification

The pet29a-TEAD2$^{217-447}$ construct was obtained from the Guo lab at the University of Texas Southwestern and transformed into the Escherichia coli strain Rosetta (DE3) to produce an N-terminal His6-tagged TEAD2$^{217-447}$. The bacteria were grown in terrific broth at 37° C with shaking at 225 RPM until an OD_{600} of about 2.0 was met. The bacteria were cooled on ice for 15 minutes and induced with 0.2 mM IPTG. Bacteria were incubated at 16° C with shaking at 225 rpm for 18 hours. Cells were collected with centrifugation at 14,000 rpm at 4° C for 15 minutes and resuspended in 2 mL lysis buffer per 1 gram of bacteria pellet (500 mM NaCl, 50 mM Tris pH 7.5, 10 mM imidazole, 5 mM beta-mercaptoethanol). Cells suspension was passed through microfluidizer four times and lysates were clarified with ultracentrifugation at 35,000 rpm at 4° C for 30 minutes, transferred to new centrifuge tubes, and spun at 35,000 RPM at 4° C for 10 minutes. Clarified lysate was filtered using a 0.45 μm disposable filter and 60 mL syringe (25mm diameter, PES membrane, GE). The filtered lysate was batch bound with buffer equilibrated Ni-NTA agarose (Invitrogen, 0.25 mL 50% resin

suspension per 50 mL lysate) with rocking on nutrator at 4° C for two hours. Lysate-resin mixture was poured into a BioRad column and washed with 40 mL wash buffer (500 mM NaCl, 50 mM Tris pH 7.5, 20 mM imidazole, 5 mM beta-mercaptoethanol) and eluted with 8 mL elution buffer (50 mM Tris pH 7.5, 500 mM NaCl, 300 mM imidazole, 5 mM beta-mercaptoethanol). Two uL of 6X sample buffer was added to 10 uL aliquots of the load, flow through, 20 mM imidazole wash, and elution fractions. The samples were boiled for 5 minutes at 95° C and loaded to a 12% acrylamide SDS gel using a Hamilton syringe. The gel was run at 200V for one hour. The gel was then Coomassie stained for visualization of proteins. Elution fractions containing TEAD2 were combined and dialyzed overnight using a Slide-A-Lyzer 10K dialysis cassette (Pierce) in 3 liters of QA buffer (20 mM Tris pH 8.5, 20 mM NaCl, 1mM DTT). Sample was loaded on an 18 mL Q Sepharose Fast Flow (GE Healthcare) packed column at a flow rate of 2.5 mL/minute. A gradient was run from 0% to 34%QB (20 mM Tris pH 8.5, 1 M NaCl, 1 mM DTT) was run over 17 column volumes and a gradient from 35% to 60%QB over 3 column volumes. Protein fractions were collected and run on a 12% acrylamide SDS gel at 200 V for one hour followed by Coomassie staining. TEAD2 containing fractions were diluted to ~20 mM NaCl and loaded to a second 18 mL Q Sepharose Fast Flow column at 2.5 mL/minute. A gradient was run from 20%QB to 36%QB over 10 column volumes. Elution fractions were run on a 12% acrylamide SDS gel at 200 V for one hour followed by Coomassie staining. Fraction contain purified TEAD2 were combined and concentrated to 4 mg/mL using a 30,000 MWCO concentrator. The concentrated protein was flash frozen with 5% v/v glycerol and 1 mM DTT and stored at -80° C.

pet29a-TEAD2$^{217-447}$: MAWQARGLGTARLQLVEFSAFVEPPDAVDSYQRHL
FVHISQHCPSPGAPPLESVDVRQIYDKFPEKKGGLRELYDRGPPHAFFLVK

FWADLNWGPSGEEAGAGGSISSGGFYGVSSQYESLEHMTLTCSSKVCSFG
KQVVEKVETERAQLEDGRFVYRLLRSPMCEYLVNFLHKLRQLPERYMM
NSVLENFTILQVVTNRDTQELLLCTAYVFEVSTSERGAQHHIYRLVRDVE
HHHHHH

2.7 Coomassie Staining

After running an SDS-PAGE gel, the gel was rinsed with water 3 times and set in 15 mL Coomassie destaining solution (40% methanol, 10% acetic acid) for 5 minutes with rocking at room temperature. The destaining solution was removed. 15 mL of Coomassie stain (0.2% Coomassie Blue R-250, 40% methanol, 10% acetic acid) was added to the gel, covered with plastic wrap, and microwaved for 10 seconds. The gel was then rocked at room temperature for 25 minutes. Coomassie blue stain was poured off and the gel was rinsed three times with water. 15 mL Coomassie destain was added to the gel, covered in plastic wrap, and microwaved for 10 seconds. Destain was replaced with fresh destain and was rocked at room temperature until bands were visible and background is clear. Several destain solution replaces were required. The stained gel was imaged on light box.

2.8 Fluorescence Polarization

10 nM fluorescently labeled peptide (5(6) FAM-YAP1$^{58-74}$ or YAP1$^{61-99}$) was incubated with TEAD2 in binding buffer (25 mM Tris pH 8.5, 250 mM NaCl, 1 mM DTT, and 5% glycerol) to a final volume of 40 uL in black Costar 384-well plates at room temperature for one hour in the dark. If testing compound effects on binding, TEAD2 was treated with compound dissolved in DMSO for 30 minutes prior to the addition of the fluorescently labeled peptide. Excitation wavelength was 485 nm and

emission was detected at 535 nm using a Cytation 1 multi-mode imaging reader (BioTek).

CHAPTER THREE: INTRACELLULAR RESULTS

3.1 Optimization and validation of a TEAD dependent transcriptional assay

A luciferase reporter assay was optimized as a precursor for the screening of the 76 compounds received from AtomWise, Inc for effects on intracellular YAP1/TEAD activity. This assay used a pGL3.1 based reporter construct that contains a 3.1 kB fragment of the *CTGF* promoter in which the serum response elements were ablated. This construct was previously demonstrated by the Wells laboratory to express firefly luciferase in direct relation to intracellular YAP1/TEAD activity. Thus, any compounds that inhibit the activation of TEAD by YAP1 will reduce the expression of firefly luciferase. Cells were simultaneously transfected with a Thymidine Kinase (TK) Renilla reniformis luciferase construct. By normalizing luciferase activity by dividing firefly activity by Renilla reniformis activity, values were corrected for differences in pipetting, transfection efficiency, and cell density. Compounds with off-target effects e.g. cellular toxicity, non-specific inhibition of transcription etc. could also be detected based upon their having significant effects on TK-Renilla activity.

Initially, three cell lines were assessed for their ability to be transfected and for significant endogenous YAP1 activity. The three cell lines included uterine cancer cells (HeLa), glioblastoma cells (A172), and kidney cells (HEK293T). Basal YAP1 activity was inferred by degree to which the TEAD reporter assay was inhibited upon silencing of YAP1. Cell lines were also evaluated for their ability to be easily transfected by the luciferase constructs. HeLa cells were both highly transfectable and had high basal levels of reporter activity. Further, this activity was inhibited by over 45 % upon transduction with transduction lentivirus encoding shRNA against YAP1. Immunoblot analysis found

an ~ 90 % reduction of YAP1 levels in cells transduced with shYAP1 relative to the control cells. (**Figure 4**). The relatively low reduction in luciferase activity upon YAP1 silencing may be due to the incomplete knockdown of YAP1 and/or the presence of other factors including TAZ that may also activate TEAD in HeLa cells. In order to determine the statistical effect size, luciferase activity was measured in 36 replicates of HeLa cells with YAP1 knockdown or shcontrol to calculate a z' factor. The result of 0.540 indicates an excellent assay (**Figure 5**).

Transfection with polyethyleneimine (PEI) was further optimized due to the low cost of this method. While the standard transfection method is performed upon cells split the day before, this resulted in poor efficiency for HeLa cells. However, the reverse transfection method, where cells are plated after splitting into media containing the PEI transfection mixture, achieved high levels of transfection and minimal cell death. This is presumably due to the ability of cells to be completely bathed in the transfection mixture before they adhere to the plate. This method was also more flexible, as cells could be split a day earlier for assays.

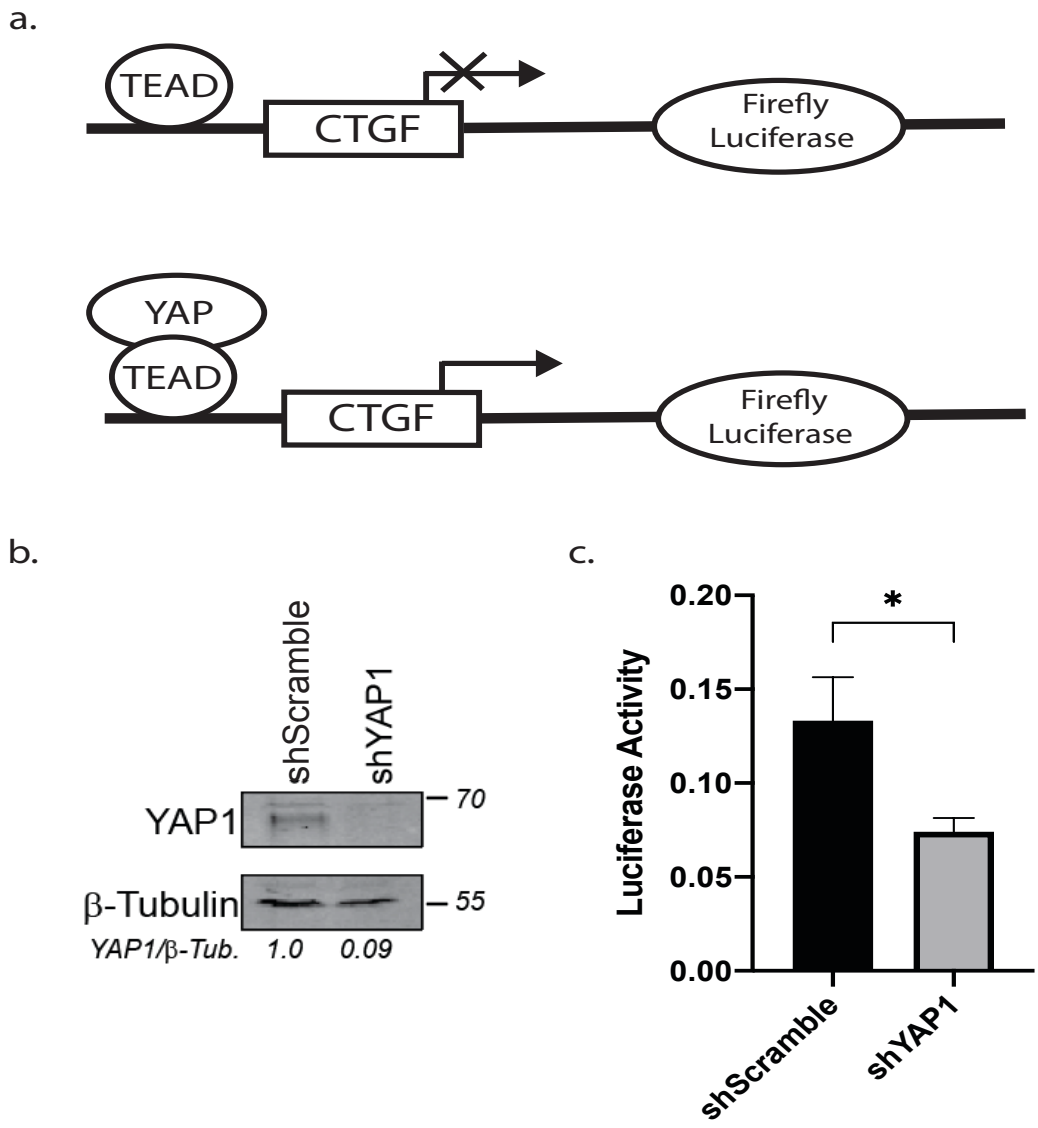

Figure 4. YAP1 dependence of the TEAD reporter assay. (a) An illustration of the luciferase reporter construct with a CTGF promoter depicts that the transcription of firefly luciferase is dependent upon the binding of the coactivator YAP1 to the transcription factor TEAD. (b) An immunoblot using the anti- YAP1 antibody and B-tubulin for a loading control demonstrates the degree of YAP1 knockdown in HeLa cells. (c) Luciferase activity (a ratio of firefly luciferase to TK Renilla) was measured in HeLa cells transduced with lentivirus with shScramble or shYAP1. N=3, *$p < 0.05$

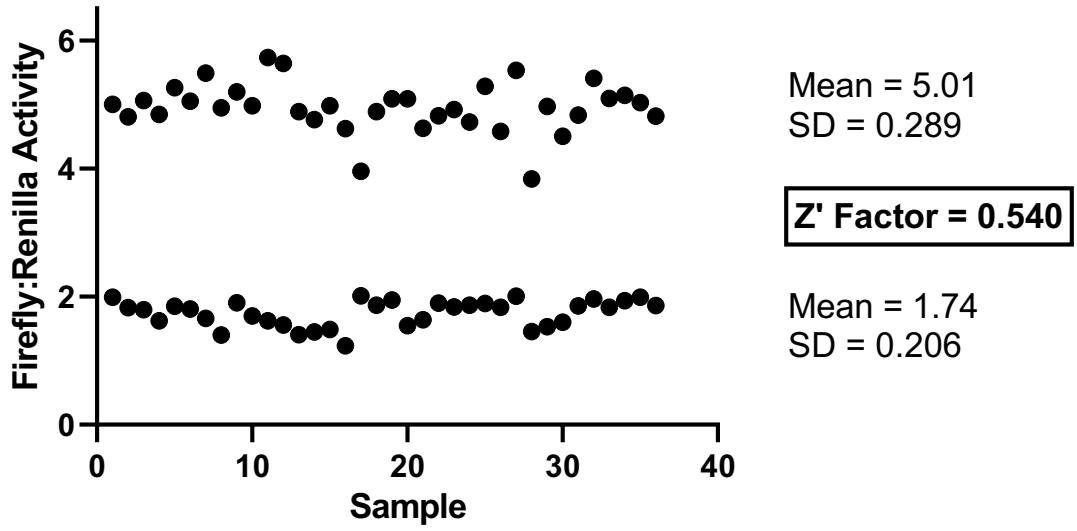

Figure 5. **The Z' factor for the TEAD reporter assay**. HeLa cells silenced for YAP1 or with control shRNA were plated into 36 replicates for each condition and TEAD reporter activity was determined. The individual activities are plotted and at right the Z' factor, overall Means, and standard deviations from the Mean are given. Z' factor was determined using the formula: $Z' = 1 - \frac{[3*(\sigma_p+\sigma_n)]}{|\mu_p-\mu_n|}$.

3.2 TEAD reporter assays and cell growth assays

The seventy-six blind compounds received from AtomWise, Inc were then screened for an ability to inhibit the TEAD reporter actvity. To this end, HeLa cells were reverse transfected with the luciferase reporter constructs and then treated with 20 μM of each compound or with vehicle for 16 hours before harvesting in passive lysis buffer. Luciferase activities were measured in lysates and are presented as the fold-difference in mean normalized luciferase values for each compound versus the normalized mean values from HeLa cells treated with vehicle (DMSO). From this data, 11 of the compounds inhibited the activity of the reporter by 50 percent or greater (**Figure 6**). Compounds showing inhibition in the reporter assay are presumed to enter the cells and the nucleus, causing a decrease in TEAD dependent transcription. Several compounds,

including **4** and **22**, inhibited the reporter activity to a greater degree than silencing YAP1 expression. However, data from compounds that exerted large effects on Renilla luciferase activity and/or resulted in significant amounts of cell death were omitted due to non-specific "denominator" effects on Renilla activity and the high intra-sample error, likely from the high levels of cell death.

In a complementary approach, Dr. Quilliam measured the effects of each compound on the viability of three cells lines (MIA PACA; pancreatic cancer, Pa14C; pancreatic cancer, and H460; lung cancer). Cell viability was determined using the MTT assay. This assay measures the degree of reduced MTT in cells by NAD(P)H-dependent oxidoreductase enzymes. Since NAD(P)H flux is mainly dependent on overall cellular metabolic activity, that, in turn, is primarily a function of cell number (assuming the treatments are over several days), this assay is very commonly used to measure cell accumulation over time. Cell viability data was combined with the TEAD luciferase reporter assay data in **Figure 7**. This highlights that while compounds **22** and **4** had the greatest TEAD luciferase reporter assay inhibition, they were not the most efficacious compounds for inhibiting cell growth. However, compound **59** was both a top 10 inhibitor of the TEAD reporter assay and it reduced cell growth by over 50 percent in two of the cell lines. In collaboration with Dr. Johnson, compounds **4**, **22** and **59** were recognized as chemically similar sulfonamides (**Figure 8**). This suggested that they may be members of a class of related compounds that target the YAP1-Phe69 binding pocket in TEAD. Compounds **4**, **22**, and **59** were therefore subjected to additional biochemical and biologic investigation.

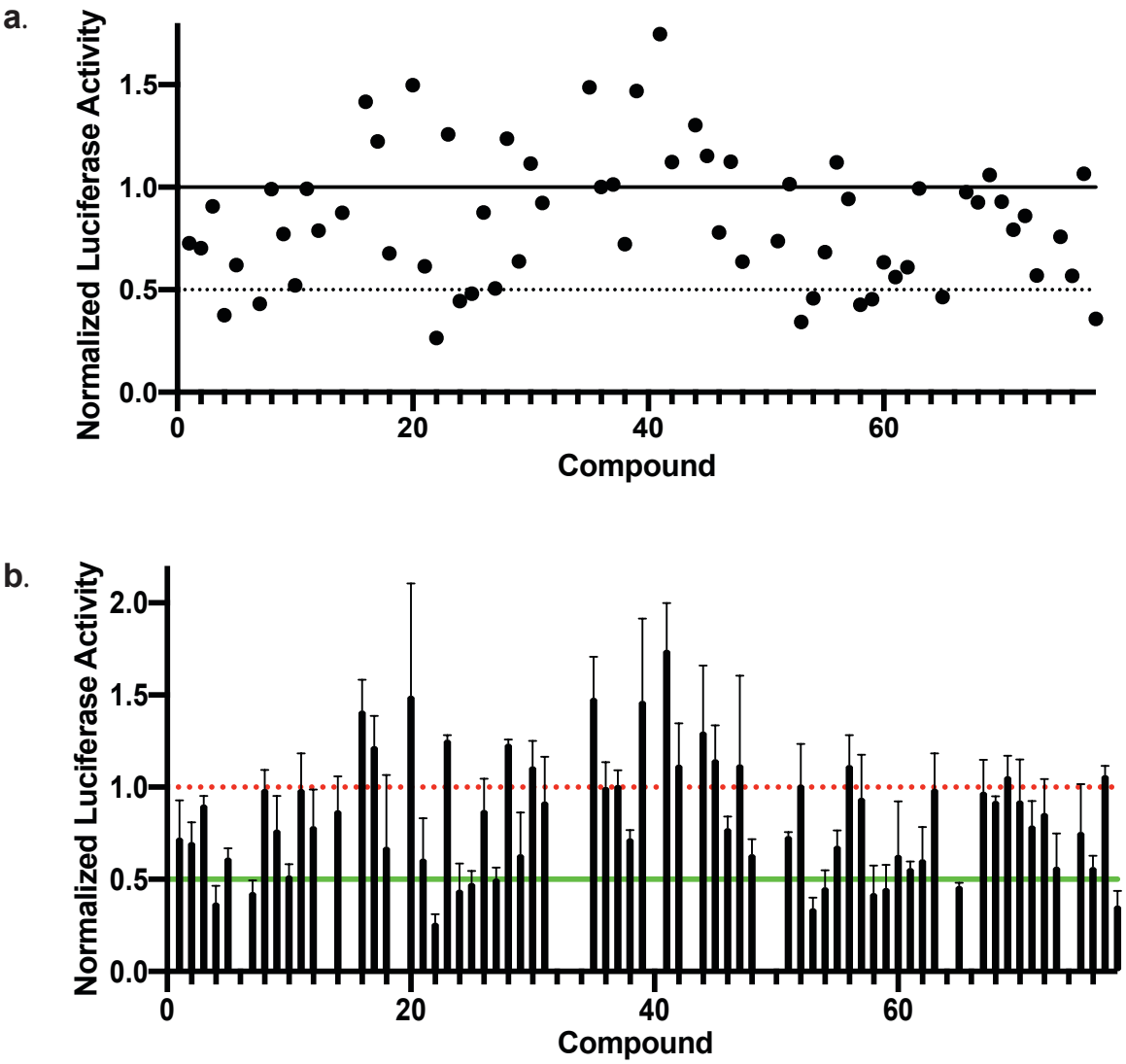

Figure 6. **Mean fold-change induced by each compound on reporter activity**. The fold-change in activities of the luciferase reporter in cells treated with each compound depicted in a scatter plot (a) and a bar graph (b). HeLa cells were treated with 20 µM of each compound and the luciferase to TK Renilla ratio was normalized to DMSO values. Each compound was tested in quadruplicate. Compounds that were toxic were omitted from the graphs. A line was included at 1.0 to emphasize the luciferase activity of cells treated with DMSO as the control.

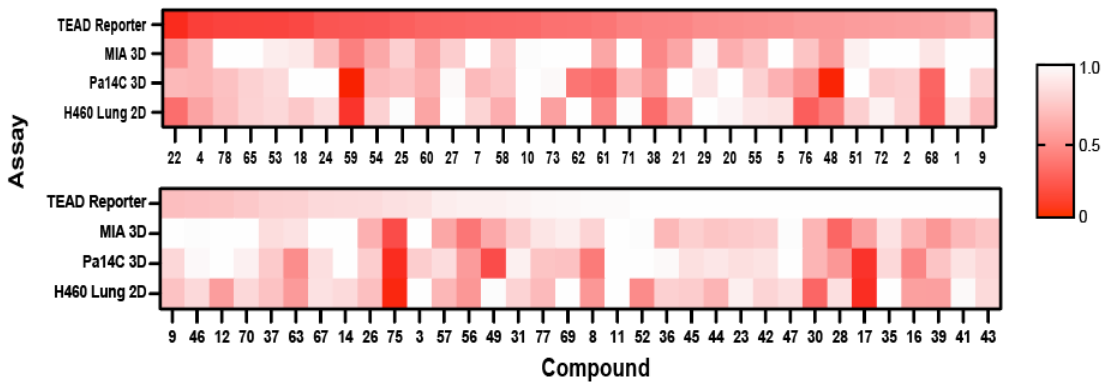

Figure 7. Association of the effects of 76 compounds on TEAD reporter activity and on cell viability. TEAD luciferase reporter assay data and cell viability data were combined into one heat map. The TEAD reporter assay data is normalized luciferase activity and the MIA, Pa14C, and H460 Lung cell viability data is in percent cell viability. The scale ranged from complete inhibition (red) to no observed inhibition (white).

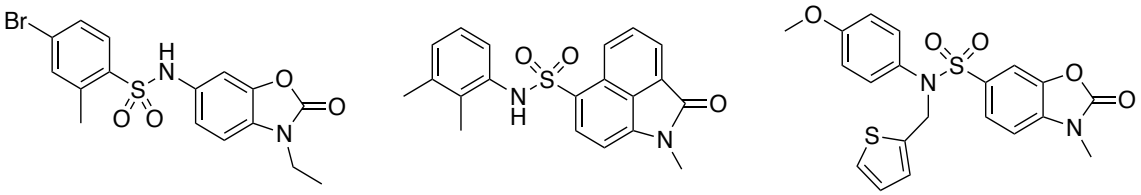

Figure 8. Structural comparison of compounds 4, 22 and 59. The similar structures, of Compounds **4**, **22**, and **59**, (all are top 10 inhibitors of the TEAD reporter assay) are depicted to highlight their common sulfonamide backbone as well as their differentiating side groups.

3.3 Structural relationships and derivatives of compounds 4, 22, and 59

The structural relationship of compounds **4**, **22**, and **59** to their activities were then probed. Compounds **4** and **59** have nearly identical substituents on one side of the sulfonamide core, but **4**, **22** and **59** have varying phenyl groups on the other side. Analogs **1989**, **1990**, **1991**, **1993**, **1994**, and **1995** were synthesized by Dr. Steven Johnson which

contain different combinations of substituents in compounds **22** and **59** (**Figure 9**). These compounds were tested for inhibition of the TEAD reporter assay. Because compound **1989** had greater inhibition than compound **59**, the aromatic-ether may inhibit binding to TEAD. While compounds **1993**, **1994**, and **1995** which contain the three ring structure of **22** had comparable levels of inhibition to compound **59** (**Figure 10**). The chemical moieties in 22 and 50 on the right side of the sulfonamide backbone may therefore bind similarly to TEAD.

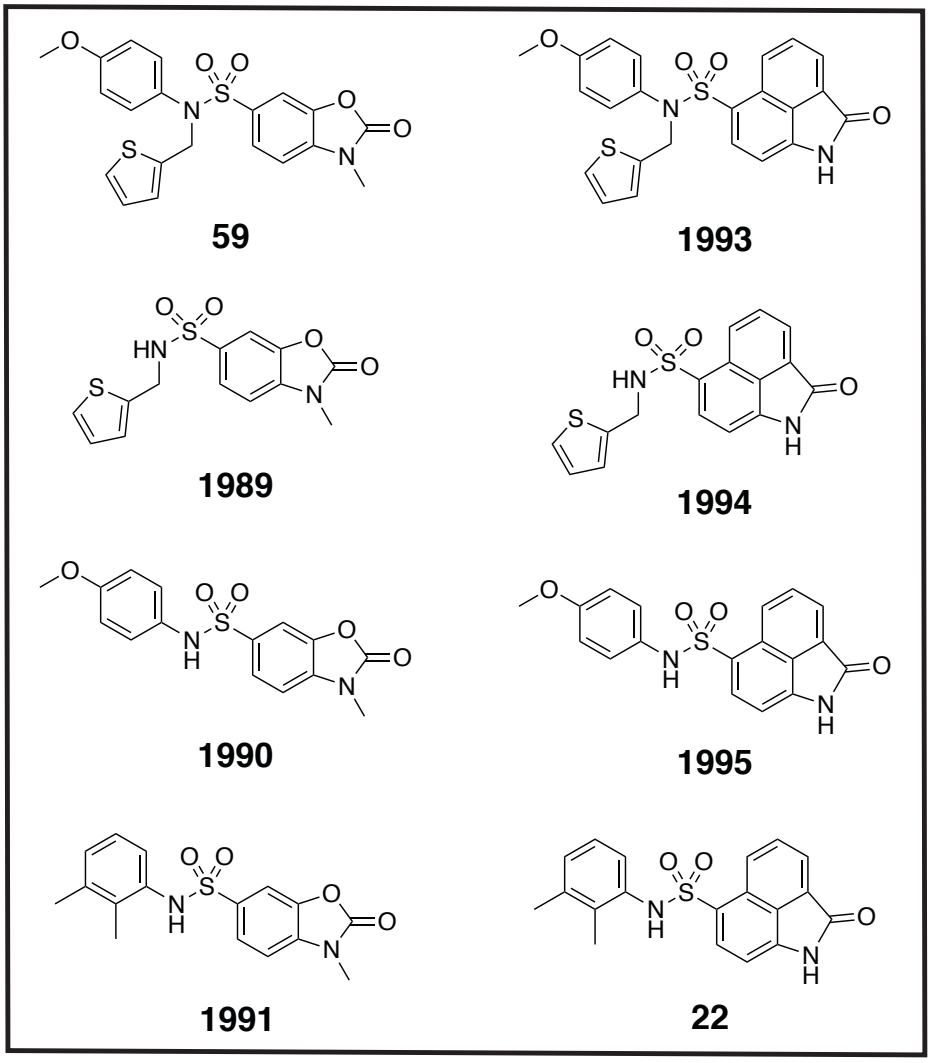

Figure 9. Structural depiction of second generation analogs. The structures of second generation analogs are shown alongside the structures of their parent compounds **4**, **22** and **59**.

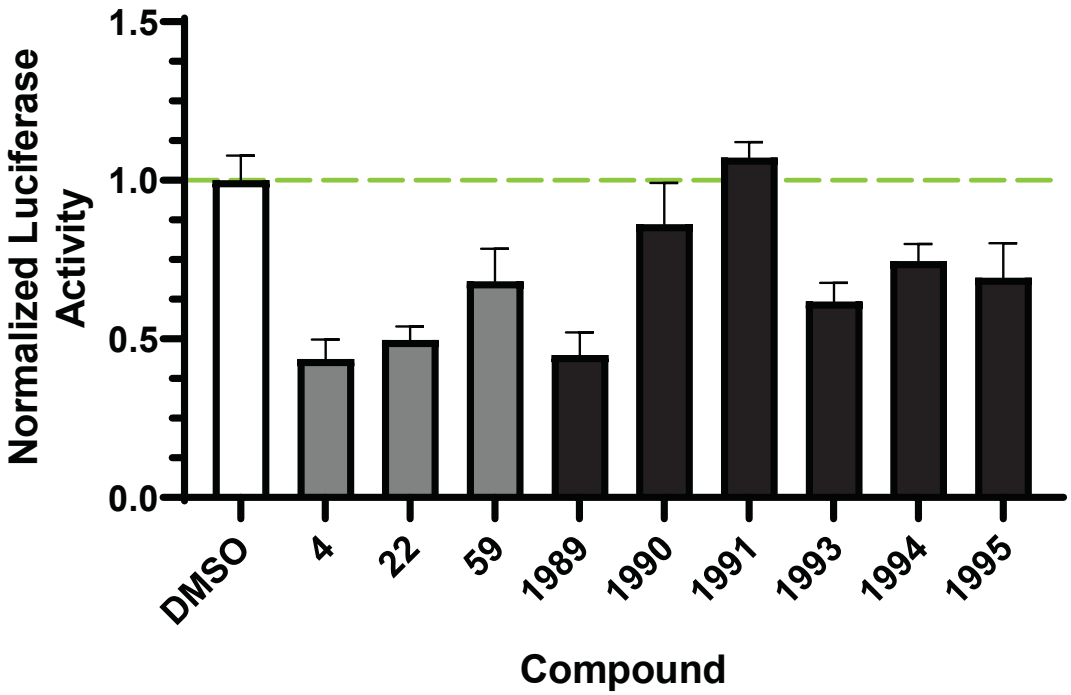

Figure 10. Mean fold-change induced by analog compounds on reporter activity. The mean fold-change of luciferase activity as a ratio of firefly luciferase to TK Renilla was measured in HeLa cells treated with 20 μM of the analogs and compounds **22**, **4**, and **59**. The luciferase activity was normalized to signal of cells treated with DMSO. Compounds were tested in quadruplicate. The line at 1.0 emphasizes the luciferase activity of the control cells treated with DMSO.

3.4 Dose response of compounds in TEAD reporter assays

Dose response curves were obtained for the effects of compounds **4, 22**, and **59** on TEAD reporter activity. Cells were treated with each compounds at concentrations from 0.3 to 30 μM in 3-fold increments. Data were then fit to nonlinear regression curves for the concentration of inhibitor vs. response with four parameters in Prism (GraphPad Inc.). IC_{50} values were then obtained using Prism for each compound. Compound **22** had the lowest IC_{50} value of 1.08 μM, followed by compounds **4** and **59**, which had IC_{50} values of 1.74 μM and 2.8 μM, respectively (**Figure 11**). Dose response curves for compounds **1989**, **1990**, **1991**, **1993**, **1994**, and **1995** (**Figure 12**), revealed that compounds **1995** and **1989** had the lowest IC_{50} values at 0.602 and 0.604 μM. Whereas the other analogs had

higher IC_{50} values than any of the original compounds on which they were based (**Table 1**).

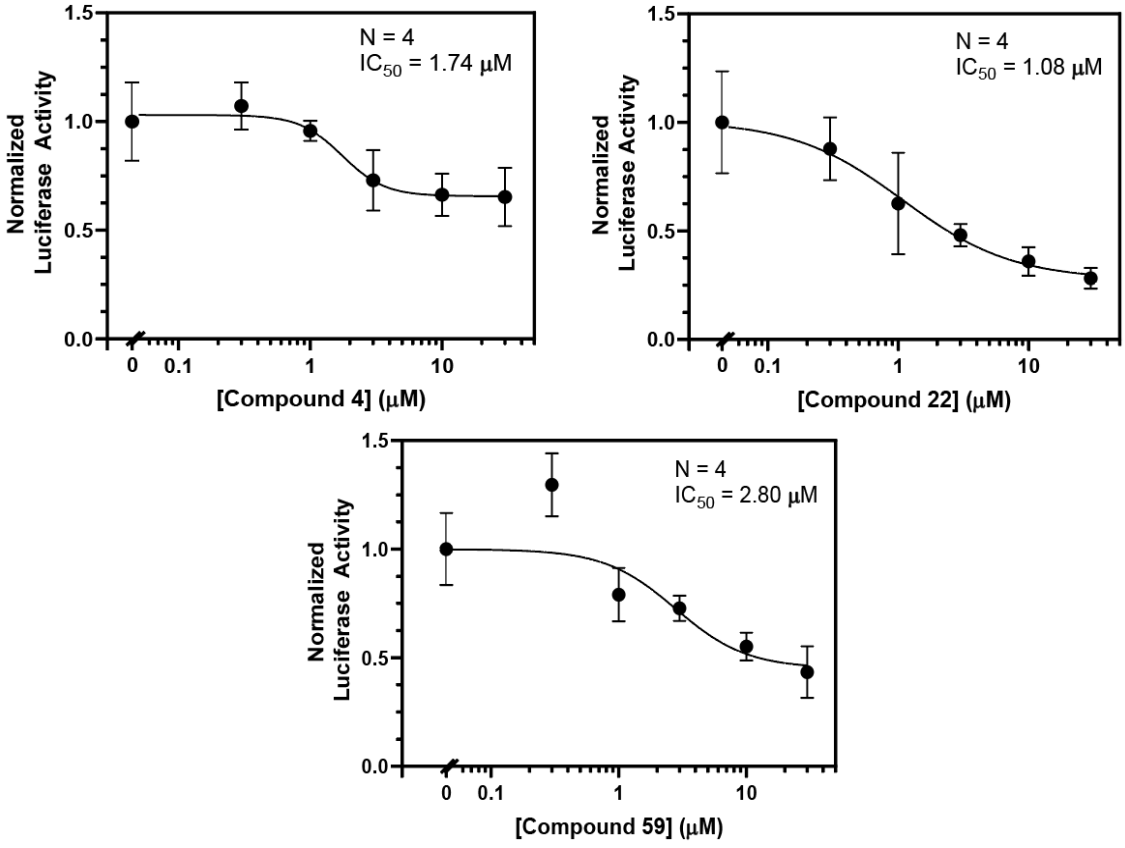

Figure 11. Dose responses of compounds 4, 22, and 59 on TEAD reporter assay. Dose response curves for compounds **4**, **22**, and **59** were obtained as a measurement of fold-change of firefly: renilla activity using the TEAD reporter assay. Nonlinear regression curves were calculated using 4 parameters with variable slope on GraphPad Prism 8 and IC_{50} values were determined based on curves. Data for individual concentrations of compounds were completed in quadruplicate.

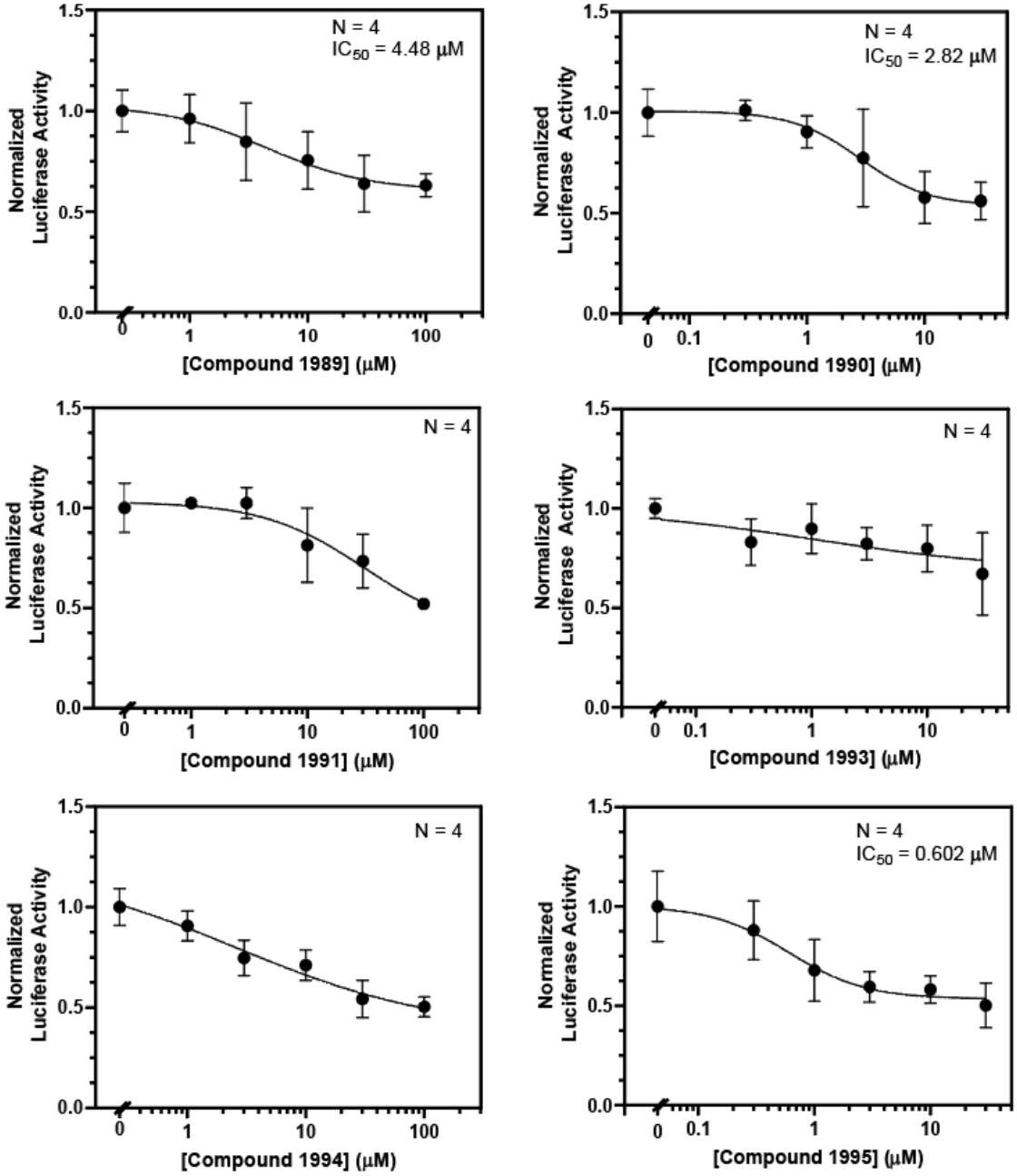

Figure 12. Dose responses of analog compounds on TEAD reporter assay. Dose response curves for the analog compounds were obtained as a measurement of fold-change of firefly: renilla activity using the TEAD reporter assay. Nonlinear regression curves were calculated using 4 parameters with variable slope on GraphPad Prism 8 and IC_{50} values were determined based on curves. Data for individual concentrations of compounds were completed in quadruplicate.

3.5 Validation of TEAD reporter inhibition with endogenous *CTGF* measurements

The impact of compounds on endogenous TEAD activity were validated by measuring their effects on the levels of endogenous *CTGF* transcript. Total mRNA was extracted from HeLa cells treated with 20 uM of compound or vehicle for 24 hours. The Relative levels of the *CTGF* transcript as well as 18S rRNA for normalization were then measured by Quantitative (q) Real-Time (RT) Polymerase Chain Reaction (PCR). *CTGF* levels in cells treated with compound **1993** were nearly 80 % lower than cells treated with DMSO, compound **4** caused a 60% decrease, and compound **22**, **1989**, and **1994** all had about a 50% decrease (**Figure 13**). However, compound no decrease in the transcription of endogenous *CTGF* was observed in cells treated with **59**. This suggests that compound 59 inhibited the TEAD reporter assay in a TEAD independent manner. All intracellular assay data for compounds 4, 22, 59, and the analogs are summarized in **Table 1**.

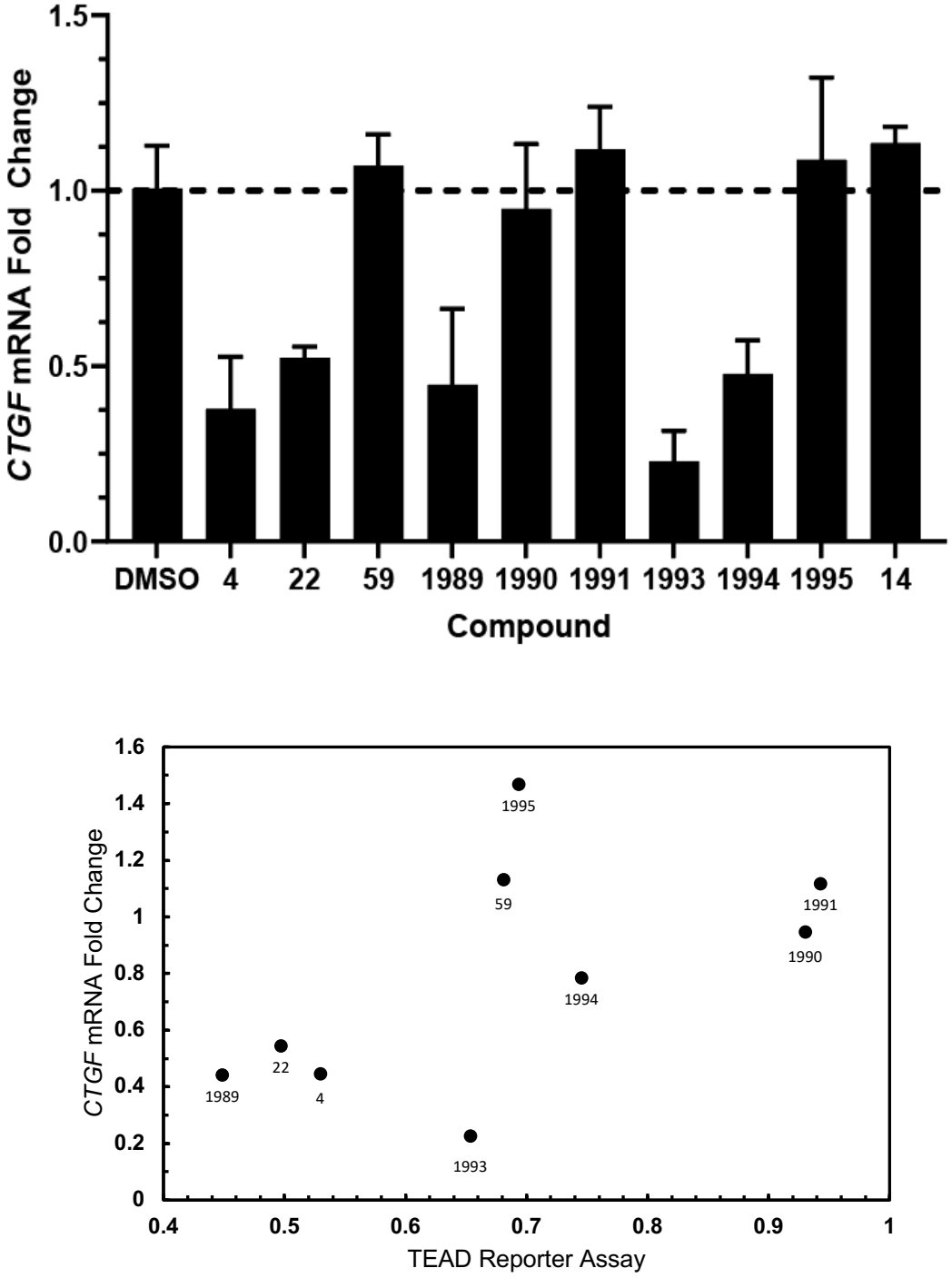

Figure 13. Validation of the ability of compounds to inhibit endogenous YAP1/TEAD activity. *CTGF* mRNA was measured through qRT-PCR in HeLa cells treated with DMSO and 20 uM of compounds. Values were normalized to 18S rRNA in the samples, N=4 (**a**). *CTGF* mRNA fold change was plotted against TEAD reporter assay data to compare artificial and endogenous *CTGF* inhibition by compounds (**b).**

Compound	IC_{50} (μM)	Highest Observed Inhibition	*CTGF* mRNA Fold Change
4	1.74	30.3%	0.447
22	1.08	71.8%	0.546
59	2.80	56.6%	1.13
1989	4.48	41.3%	0.443
1990	2.82	43.9%	0.948
1991	N/A	57.8%	1.12
1993	N/A	38.2%	0.227
1994	N/A	51.9%	0.786
1995	0.602	45.5%	1.47

Table 1. Summary of intracellular assay data. IC_{50} values reported from TEAD reporter dose response curves, the highest observed inhibitions seen in TEAD reporter dose response curves, and *CTGF* mRNA fold change data for each compound.

3.6 Cell growth of PKD cells treated with compound 22

In collaboration with the Bacallao Lab, the effects of compound 22 were determined on the growth of autosomal dominant polycystic kidney (ADPKD) cells, healthy kidney cells from and ADPKD patient (adjacent ADPKD), and normal kidney cells treated. While compound 22 inhibited the growth of PKD cells by 20 percent, it had no effect on the growth of normal kidney cells or matched normal adjacent cells taken from an ADPKD patient (**Figure 14**). Compound 22 may therefore hold promise as the basis for a PKD therapeutic because it prevents the growth of ADPKD cells but not healthy kidney cells.

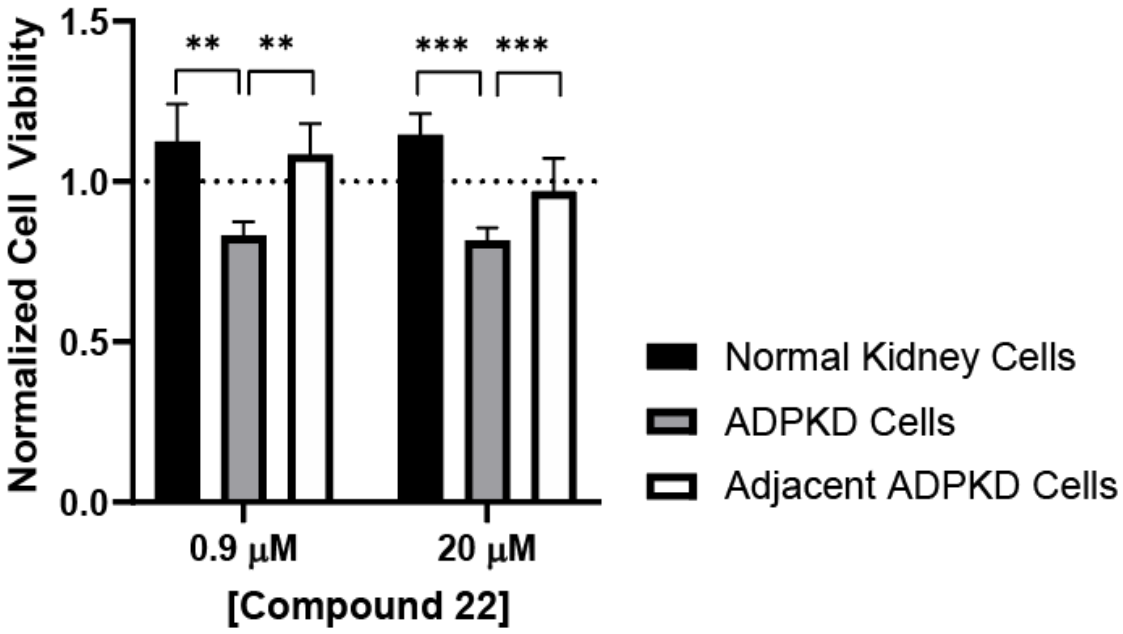

Figure 14. Metabolic effects of compound 22 on ADPKD cells. Cell growth of normal kidney, autosomal dominant polycystic kidney disease (ADPKD), and adjacent autosomal dominant polycystic kidney disease cells treated with 0.9 and 20 uM compound 22 for 36 hours were measured through an MTT assay and normalized to cells treated with DMSO. Samples were completed in quadruplicate. *** $p < 0.001$, ** $p < 0.01$.

CHAPTER FOUR: BIOCHEMICAL RESULTS

4.1 Validation of the identity and purity of compounds acquired from AtomWise

The purity and identify of 16 compounds with the greatest effect on the TEAD reporter were validated by HPLC and LC-MS (performed by Dr. Steven Johnson and Mckayla Stevens, IUSM). The results from these analyses are summarized in **Table 2** alongside their expected masses. The purity of compounds 4, 22, and 59, were all > 97%, and the masses of compounds 4 and 22 matched expected values. However, the mass measured for compound 59 did not match the expected value. Compound 59 was consequently re-synthesized by Dr. Johnson and shown to have the same "incorrect" mass by LC-MS. The lack of a good ionizing group on compound 59 may prevent it from flying well in the MS. Consequently, compound 59 was analyzed by both H^1 NMR and C^{13} NMR, which both supported a correct structure.

Compound	HPLC-1 (Acetonitrile)	HPLC-2 (Methanol)	MS Obtained	MS Expected
4	**99%**	**98%**	**408.9**	**409.0**
7	>99%	99%	465.9	429.9
10	>99%	>99%	405.1	405.2
18	96%	96%	446.0	446.1
22	**97%**	**>99%**	**365.0**	**365.1**
24	87%	86%	445.1	445.2
25	>99%	>99%	378.0	378.1
27	97%	99%	407.0	407.1
53	98%	>99%	406.0	406.1
54	78%	78%	442.1	442.1
58	99%	98%	400.1	400.1
59	**>99%**	**>99%**	**461.0**	**429.1**
61	68%	98%	440.0	440.1
62	>99%	>99%	408.9	409.0
73	92%	96%	401.0	401.2
78	>99%	>99%	371.1	371.1

Table 2. **Validation of identity and purity of compounds through mass spectrometry and HPLC.** The identity and purity of compounds received from AtomWise, Inc were

validated through HPLC with methanol and acetonitrile as solvents and mass spectrometry.

4.2 TEAD2 expression and purification

Initial attempts to purify TEAD employed a Yeast expression system to potentially increase the amount of TEAD with palmitoylation. After several attempts of expressing and purifying TEAD in yeast, we became aware that the strain provided by our yeast collaborator did not contain recombinant TEAD. All consequent efforts to purify TEAD utilized *E. coli* for expression.

A 6x His-tagged TEAD2 cDNA (obtained from Guo at University of Texas Southwestern) was obtained as this construct was used to express proteins that were consequently used to obtain x-ray crystallography structures. Purified TEAD2 was auto-palmitoylated by incubation with palmitoyl-CoA. Quadrupole-time of flight mass spectroscopy (QToF) (completed by Dr. Georgiadis) confirmed that a majority of TEAD2 was palmitoylated. As seen in **Figure 15**, non-palmitoylated TEAD2 with a mass of 27321.9 g/mol and palmitoylated TEAD2 at a mass of 27560.5 g/mol are both highly represented. Specifically, 31.5% of the TEAD2 was palmitoylated before incubation with palmitoyl-COA, whereas 63.8% of the TEAD2 was palmitoylated after incubation with palmitoyl-CoA (**Table 3**).

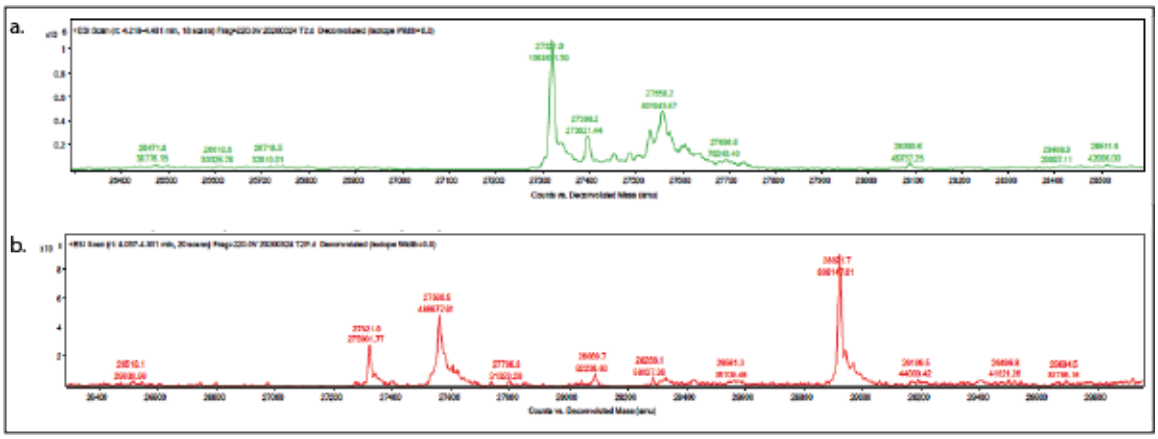

Figure 15. Mass spectrometry analysis of TEAD2 treated with palmitoyl-CoA. QToF was used to validate that TEAD2 was expressed and purified and to determine the amount of unpalmitoylated and palmitoylated TEAD2 in both the unmodified sample (a) and the sample with added Palmitoyl CoA (b). Unpalmitoylated TEAD2 has a mass of 27321.9 g/mol and palmitoylated TEAD2 has a mass of 27560.6 g/mol.

Unmodified TEAD2				**Palmitoylated TEAD2**		
Mass (g/mol)	Area Under Curve	Percent of Total TEAD		Mass (g/mol)	Area Under Curve	Percent of Total TEAD
27321.9	1068611.39	68.5%		27321.9	275901.77	36.2%
27560.5	491943.57	31.5%		27560.5	486977.91	63.8%

Table 3. Mass spectrometry analysis of TEAD2 treated with palmitoyl-CoA. The abundancies of unpalmitoylated TEAD2 (mass of 27332.9 g/mol) and palmitoylated TEAD2 (mass of 27560.5 g/mol) were determined for the purified TEAD2 before and after the addition of palmitoyl-CoA using QToF.

4.3 Fluorescence polarization

Two YAP1 peptides were synthesized (Dr. Mark Jarosinski) consisting of the residues 58-74 (Peptide#1) or residues 61-99 (Peptide#2) from full-length YAP1. Peptide#1 contains the residues that make up the alpha-helical region of YAP1 that binds to TEAD. Peptide#2 contains all of the residues in the three interfaces that bind to TEAD. Fractions of both peptides were coupled to 6-carboxyfluorescein (5(6)-FAM) at their N-termini for use in fluorescence polarization studies.

The binding of these two YAP1 peptides to purified TEAD were then measured by fluorescence polarization based studies. We first investigated whether the palmitoylation of TEAD2 affects its binding to the YAP1 peptides. While non-palmitoylated TEAD2 had no detectable binding to Peptide#1, it bound to peptide #2 with a similar Kd as palmitoylated TEAD2 (**Figure 16**). The binding of fluorescently labeled peptide #1 to palmitoylated TEAD was then measured in backgrounds of increasing concentrations of unlabeled peptide #1 (**Figure 17**). The small decrease in fluorescence polarization observed at higher concentration of unlabeled peptide suggests that changes in fluorescence polarization values reflects some degree of specific binding of YAP1 to TEAD. The impact of increasing concentrations of compounds 4, 22, 59, and 78 on the binding of fluorescently labeled YAP1 peptide #2 to TEAD were then completed (**Figure 18**). While compound #4 had no effect even at 30 uM, a modest decrease in YAP1 binding to TEAD was observed in the presence of 1 to 30 μM of compounds 4, 22 and 59. Similar dose response curves for compounds 1989, 1990, 1991, 1993, 1994, and 1995 revealed that compounds 1991 and 1994 at 1- 30 μM showed significant reduction of YAP1 binding to TEAD (**Figure 19**). In summary, compounds

22, 1991, and 1994 have predicted IC_{50} values of 9.07, 1.75, and 6.66 μM, while all other compounds had little to no effect.

While these data have made important steps for biochemically measuring the ability of compounds to inhibit YAP1 binding to TEAD, there are still several experimental issues to be resolved. Important accomplishments include the development of an optimized protocol to purify TEAD as well as preparation of several milligrams of highly purified TEAD. Further, we have designed and synthesized Peptide#2, which by fluorescence polarization appears to bind to TEAD with submicromolar affinity. However, many issues must be resolved to complete these studies. This includes increasing the dynamic range over which FP values change in response to increasing concentrations of YAP1 peptide #2. While, a range of 0.1 units is observed, a range of 0.25 units from roughly 0.05 to 0.3 is generally found in similar types of studies [53]. This may be improved by increasing the amount of TEAD in these assays from 1 μM to 3 μM. Further, assays examining the ability of compounds to compete with YAP1 for binding to TEAD had low precision and the inhibition of YAP1 binding was modest. These issues may be improved by using preparations of TEAD that are more pure and or stable. Also, the fluorophore on the YAP1 peptides may have suffered from photobleaching. This may be improved by making new solutions of peptide from powdered stocks and by preparing the assays for fluorescence polarization under low light levels.

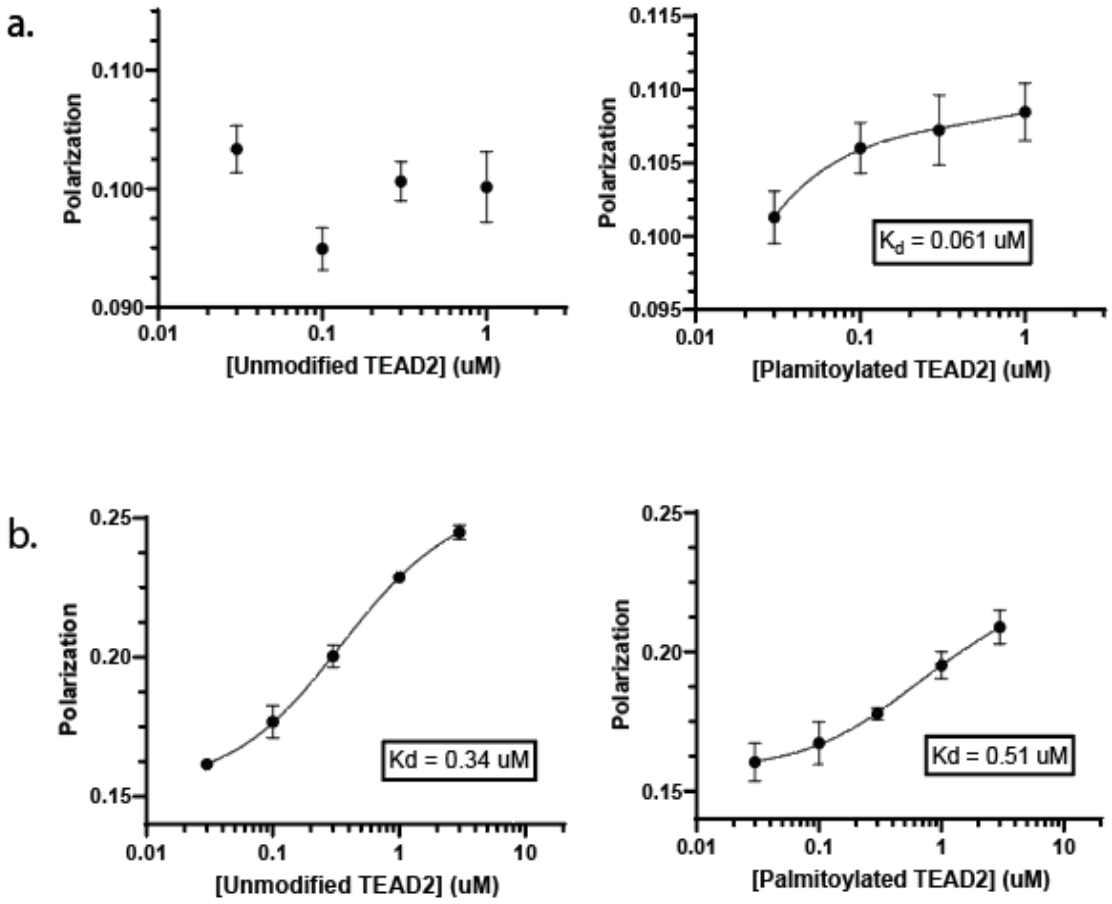

Figure 16. Binding effects of YAP1 to TEAD2 upon palmitoylation of TEAD2. Fluorescence polarization was used to analyze the binding of peptide #1 (a) and peptide #2 (b) unmodified TEAD2 and TEAD2 treated with palmitoyl-CoA. 10 nM of fluorescently labeled peptide was used with increasing concentrations of palmitoylated TEAD2 and unmodified TEAD2. Samples were completed in quadruplicate.

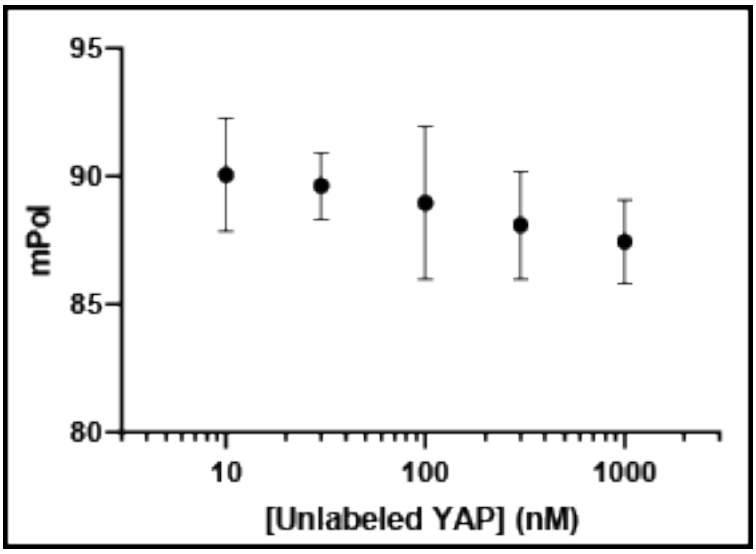

Figure 17. Competitive binding curve of YAP1 fluorescently labeled peptide #1 and unlabeled peptide #1 with TEAD2. A competitive binding curve using 10 nM fluorescently labeled Peptide#1 and increasing concentrations of unlabeled peptide #1 was completed using fluorescent polarization. N=8

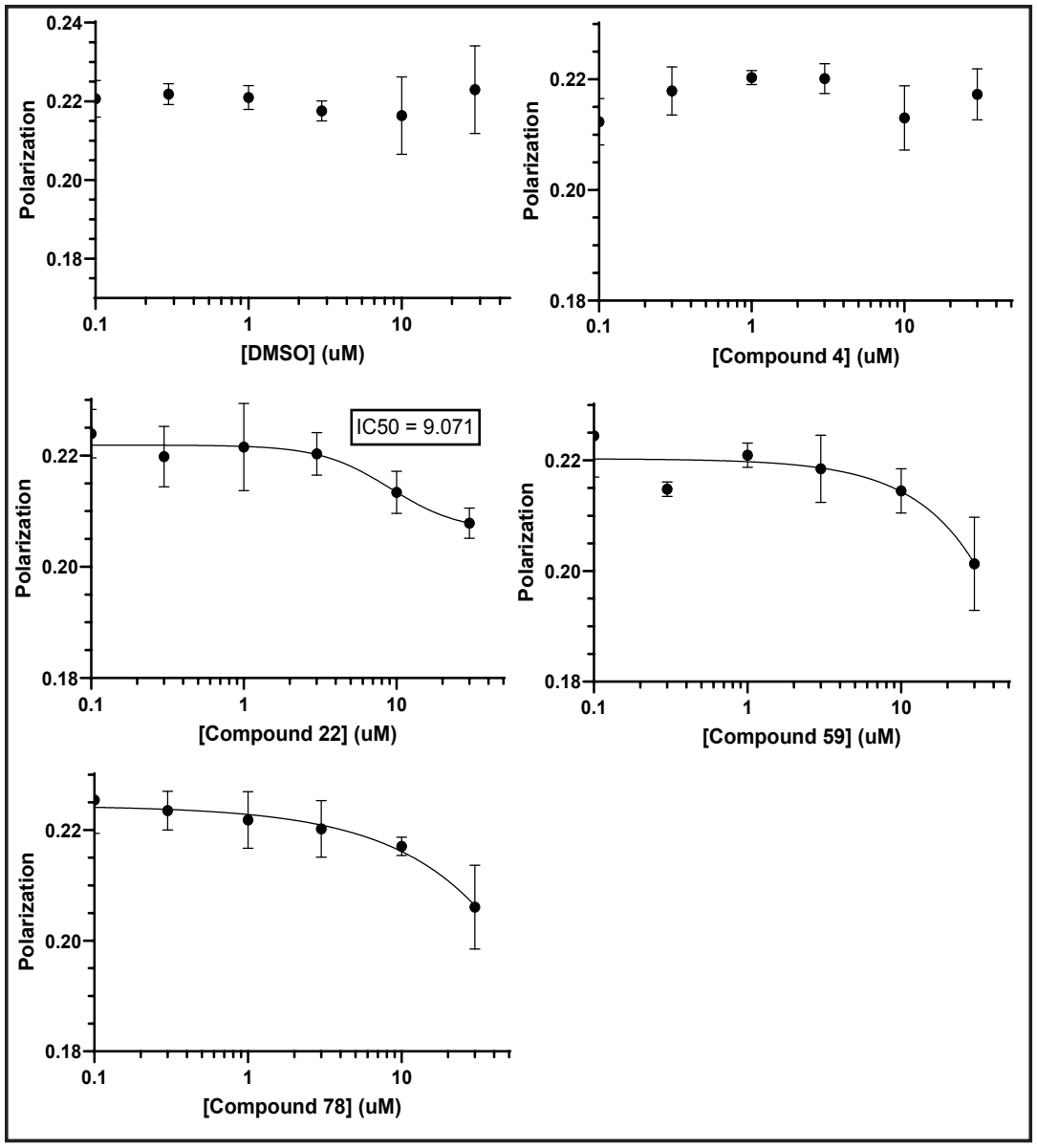

Figure 18. Effects of compounds 4, 22, 59, and 78 on peptide #2 binding with TEAD2. Dose responses of compounds 4, 22, 59, and 78 were completed by fluorescence polarization using 1 uM of palmitoylated TEAD2 and 10 nM fluorescent peptide #2. GraphPad Prism8 was used to fit curves and determine IC_{50} values using 4 parameters and a variable slope. N=4

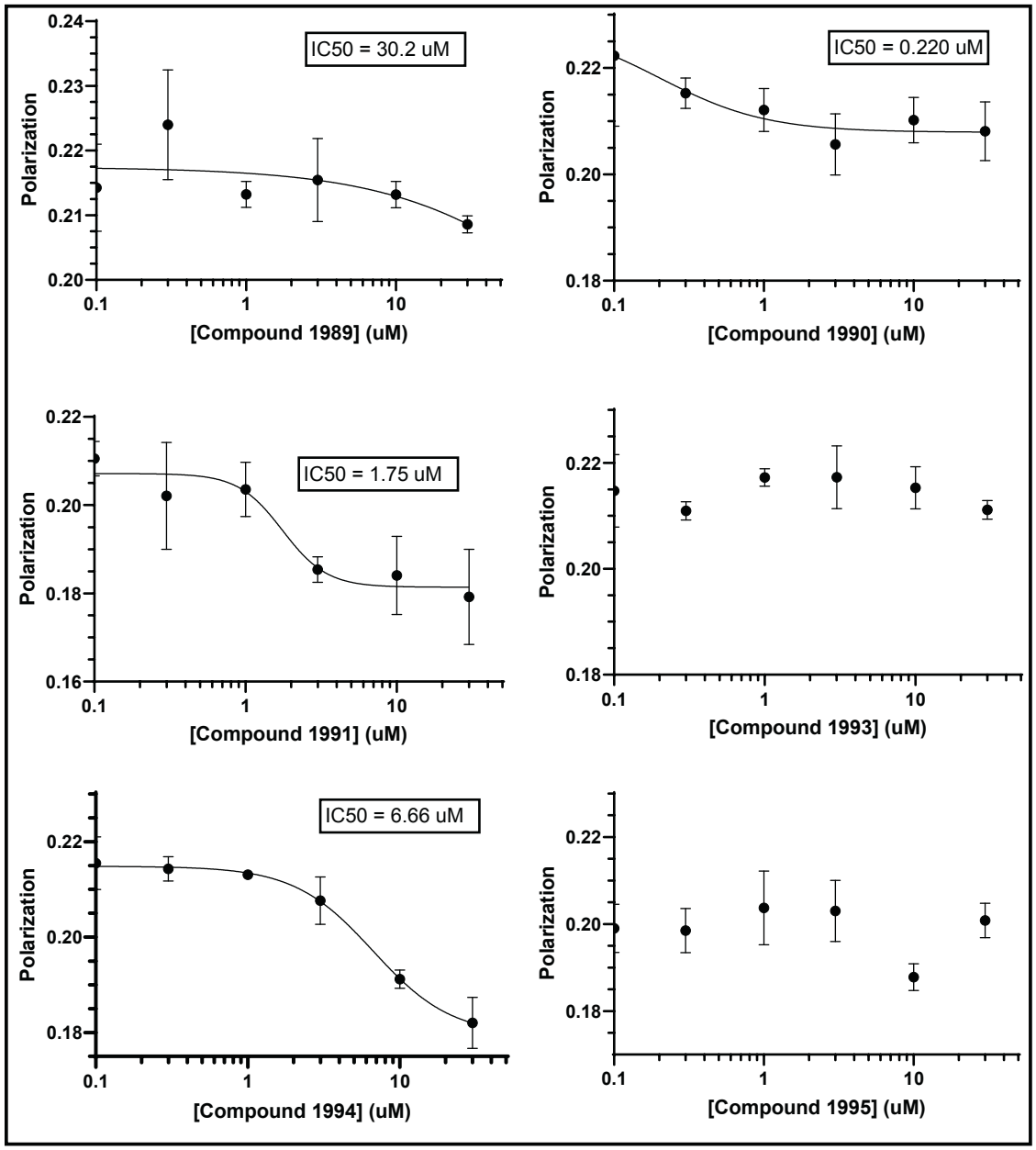

Figure 19. Effects of analog compounds on peptide #2 binding with TEAD2. Dose responses of compounds 1989, 1990, 1991, 1993, 1994, and 1995 were completed by fluorescence polarization using 1 uM of palmitoylated TEAD2 and 10 nM of fluorescent peptide #2. GraphPad Prism8 was used to fit curves and determine IC_{50} values using 4 parameters and a variable slope. N=4

CHAPTER FIVE: DISCUSSION

5.1 Compounds 22 and 59 as YAP1:TEAD inhibitors

Increased levels of YAP1 have been linked to cellular proliferation, de-differentiation and cell survival to drive tumor progression and spreading. By preventing the binding of the coactivator YAP1 to the transcription factor TEADs, the initiation and metastasis of cancer could be prevented. Several studies report small molecules that inhibit the binding of YAP1 to TEAD but none of these reagents have been shown to possess high specificity and promising anti-tumor action. This work has shown that compounds 22 and 59 both inhibit TEAD dependent transcription and cell growth in multiple cancer cell lines making them promising inhibitors of YAP1-TEAD interactions. Further, preliminary data suggests that several of the compounds physically inhibits the binding of YAP1 to TEAD. The relatedness of these compounds opens up the potential for rational design of improved compounds that may lead to the discovery of a potent YAP1:TEAD inhibitor.

5.2 Compound 22 as a potential PKD therapeutic

ADPKD cells that were treated with compound **22** for 24 hours exhibited a 20% decrease in cell growth, while adjacent ADPKD cells and healthy kidney cells saw no decrease in cell growth when treated with compound **22** for the same amount of time. This is an exciting result, suggesting that the ADPKD cells are growing in a YAP1/TEAD dependent manner and the healthy cells, even in an ADPKD patient, are not affected with treatment of compound **22**. A complete dose response curve will need to be completed with compound **22** and ADPKD cells, but the fact that the ADPKD cells

had 20% growth inhibition when treated with both 0.9 uM and 20 uM of compound **22** suggests that 20% inhibition may be the greatest inhibition that can be seen through a YAP1:TEAD inhibitor. This may be because only a fraction of the kidney cells of an ADPKD patient actually possess the *Pkd1* mutation that leads to accumulation of nuclear YAP1. This means only a small portion of the cells are growing due to increased nuclear YAP1, so seeing growth inhibition even at 20% is promising.

5.3 Sulfonamides as potential YAP1:TEAD binding inhibitors

The initial screen of compounds received from AtomWise, Inc revealed that the compounds that caused the largest decrease in TEAD dependent transcription are all sulfonamides. Sulfonamides have been widely studied and used as antimalarial and antibacterial agents. Because sulfonamides have been used for treatment of human disease, they are intriguing in research due to sufficient absorption, distribution, metabolism, and excretion (ADME) properties that have been seen in several other sulfonamides. Sulfonamides are also easy to synthesize, allowing for the creation of a large library of sulfonamides to be tested. This work touched on the possibilities of SAR by synthesizing and analyzing the activity of six chemical analogs of the inhibitors initially screened. This expanded on the moieties of the compounds initially observed to have the largest effects on TEAD dependent transcription, including compounds 4, 22, and 59, which all had amide bond containing rings. Because the initial assay was completed intracellularly, we know that these compounds are permeable to the cell membrane. This also suggests that these compounds are permeable to the nuclear membrane because it is having an effect on TEAD dependent transcription, making these

sulfonamide compounds even more interesting. Further SAR work can be done by making a larger library of compounds, adjusting the substituents and moieties based on data obtained on the activity of the compounds.

5.4 The role of palmitoylation of TEAD2 in YAP1:TEAD interactions

To date, it has been controversial whether the palmitoylation of TEAD is necessary for its binding ability and function. Fluorescence polarization data in this work suggests that the palmitoylation of TEAD2 may play a role in the stability and structure of the alpha helical region of the TEAD2:YAP1 binding domain that contains the hydrophobic pocket, which interacts with the YAP Phe-69. However, the 38 amino acid peptide that interacts with the alpha helical, beta strand, and omega loop of TEAD2, bound similarly to palmitoylated and unmodified TEAD2. In fact, unmodified TEAD2 seems to bind with a slightly higher affinity to the longer peptide. However, this could be due to the palmitoylated TEAD2 being less pure. On the other hand, the short peptide appears to only bind the palmitoylated TEAD2 and does not bind unmodified TEAD2. This data suggests that the palmitoylation within the deep hydrophobic pocket of TEAD2 plays an important role in the folding and stability of the region within TEAD that binds to the alpha helical region of YAP1.

5.5 Future Work with YAP:TEAD inhibitors

This work has shown that compound 22 is a promising inhibitor of intracellular YAP-TEAD and that it possess a modest ability to disrupt YAP1 binding to TEAD in a purified system. While the FP data is preliminary, compounds 1991 and 1994 were

actually more effective inhibitors of YAP1 binding to TEAD than either 22 or 59. However, these analogs had a poorer ability to disrupt the intracellular activation of TEAD by YAP1. Consequently, additional FP experiments will be needed to fully characterize the biochemical potential of these compounds to disrupt YAP1 binding to TEAD. Because a decrease in binding to the fluorescently labeled peptide was not seen in the presence of increasing concentrations of unlabeled peptide, the fluorescent polarization assay used in this work is not working properly. It is possible that the FAM fluorophore is interacting with TEAD2 not in the protein binding domain. In the future, a new fluorophore could be attached to the peptide to see if a better competitive binding curve can be seen. Future work using x-ray crystallography could also show how these compounds bind to TEAD2 which will enable further structure-activity relationships (SAR). A long-term goal would be the development of compounds that have efficacy in animal models of certain cancers. This would then lay the groundwork for moving these compounds forward in drug development to improve patient outcomes.

APPENDIX

Compounds received from AtomWise, Inc

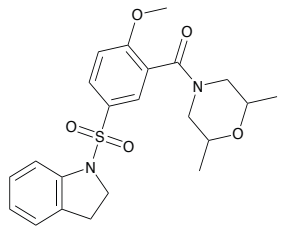 Compound 1	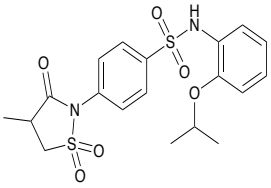 Compound 2	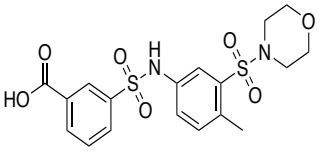 Compound 3
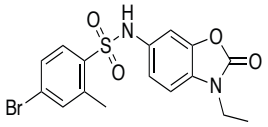 Compound 4	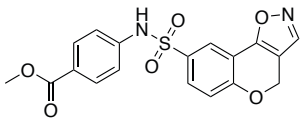 Compound 5	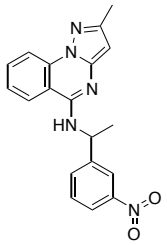 Compound 6
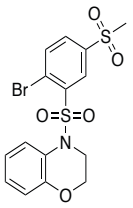 Compound 7	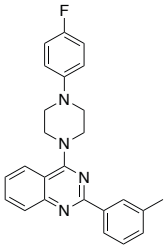 Compound 8	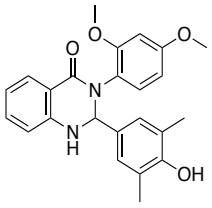 Compound 9
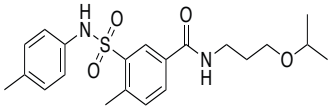 Compound 10	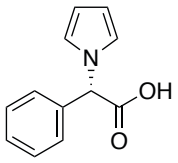 Compound 11	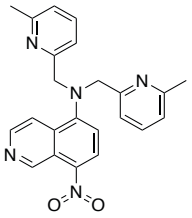 Compound 12

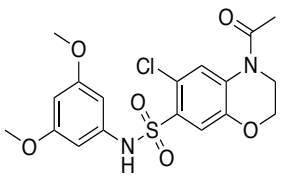 Compound 13	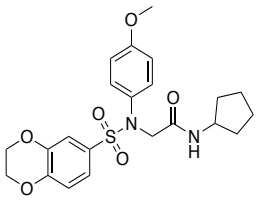 Compound 14	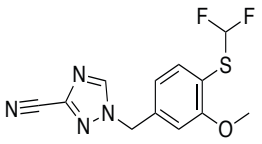 Compound 15
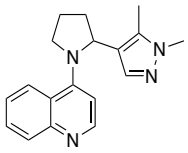 Compound 16	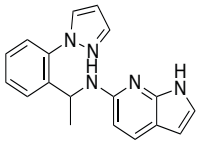 Compound 17	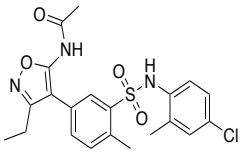 Compound 18
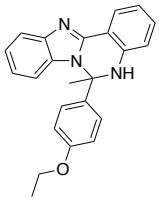 Compound 19	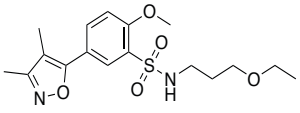 Compound 20	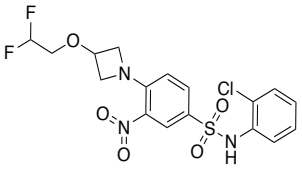 Compound 21
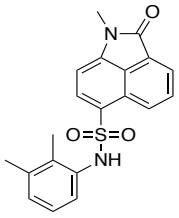 Compound 22	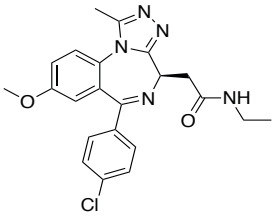 Compound 23	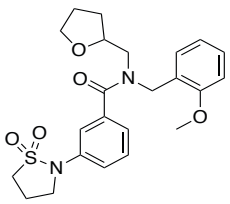 Compound 24
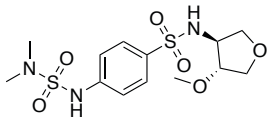 Compound 25	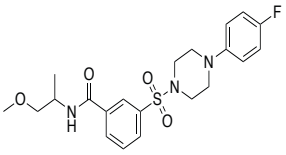 Compound 26	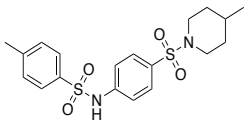 Compound 27

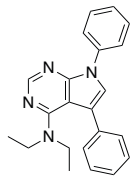 Compound 28	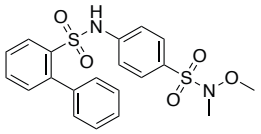 Compound 29	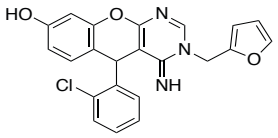 Compound 30
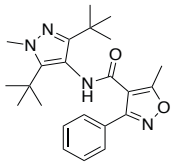 Compound 31	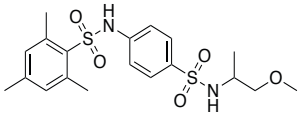 Compound 32	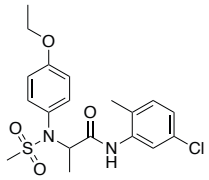 Compound 33
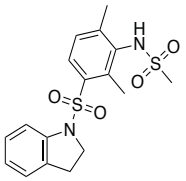 Compound 34	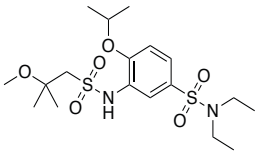 Compound 36	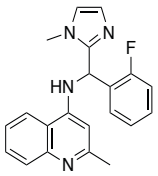 Compound 37
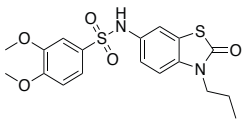 Compound 38	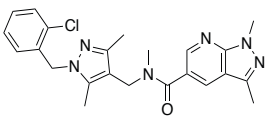 Compound 39	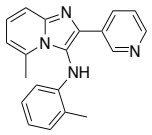 Compound 40
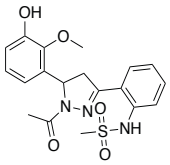 Compound 41	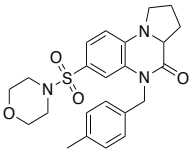 Compound 42	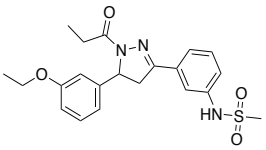 Compound 43
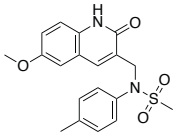 Compound 44	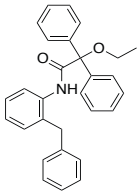 Compound 45	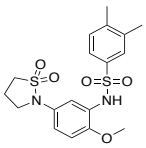 Compound 46

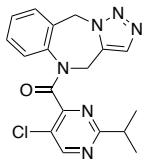 Compound 47	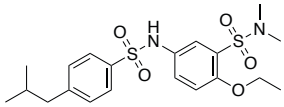 Compound 48	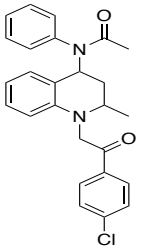 Compound 49
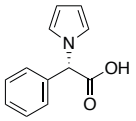 Compound 50	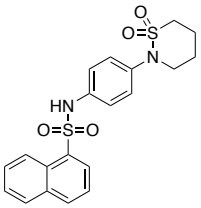 Compound 51	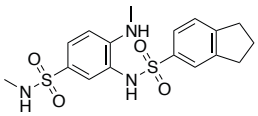 Compound 52
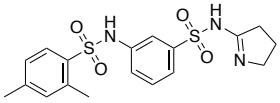 Compound 53	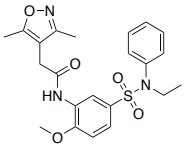 Compound 54	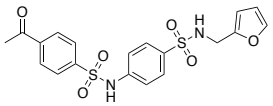 Compound 55
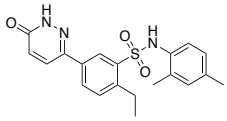 Compound 56	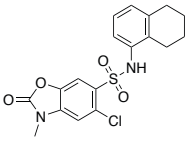 Compound 57	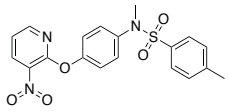 Compound 58
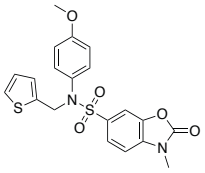 Compound 59	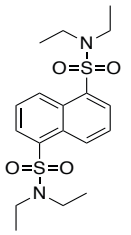 Compound 60	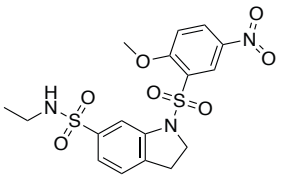 Compound 61
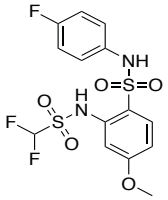 Compound 62	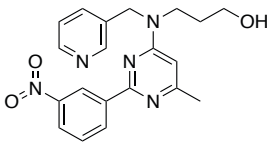 Compound 63	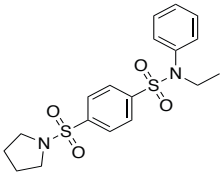 Compound 64

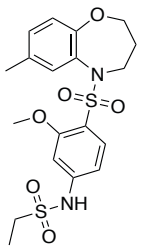 Compound 65	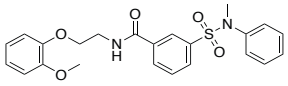 Compound 66	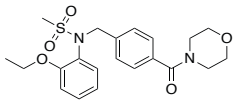 Compound 67
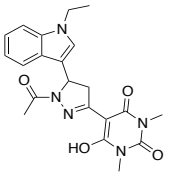 Compound 68	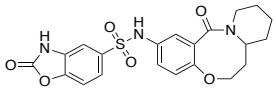 Compound 69	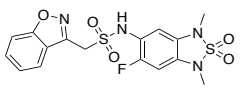 Compound 70
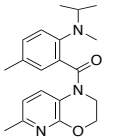 Compound 72	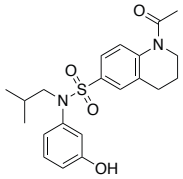 Compound 73	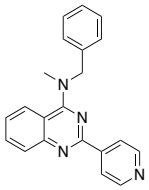 Compound 74
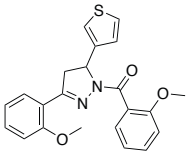 Compound 75	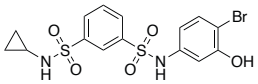 Compound 76	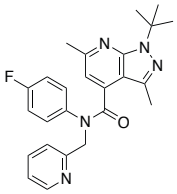 Compound 77
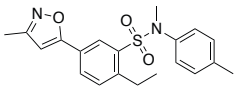 Compound 78		

REFERENCES

1. Yu, F.X., B. Zhao, and K.L. Guan, *Hippo Pathway in Organ Size Control, Tissue Homeostasis, and Cancer.* Cell, 2015. **163**(4): p. 811-28.
2. Gumbiner, B.M. and N.G. Kim, *The Hippo-YAP signaling pathway and contact inhibition of growth.* J Cell Sci, 2014. **127**(Pt 4): p. 709-17.
3. Chakraborty, S. and W. Hong, *Linking Extracellular Matrix Agrin to the Hippo Pathway in Liver Cancer and Beyond.* Cancers (Basel), 2018. **10**(2).
4. Meng, Z., T. Moroishi, and K.L. Guan, *Mechanisms of Hippo pathway regulation.* Genes Dev, 2016. **30**(1): p. 1-17.
5. Zhao, B., et al., *Inactivation of YAP oncoprotein by the Hippo pathway is involved in cell contact inhibition and tissue growth control.* Genes Dev, 2007. **21**(21): p. 2747-61.
6. Abylkassov, R. and Y. Xie, *Role of Yes-associated protein in cancer: An update.* Oncol Lett, 2016. **12**(4): p. 2277-2282.
7. Lin, K.C., et al., *Regulation of Hippo pathway transcription factor TEAD by p38 MAPK-induced cytoplasmic translocation.* Nat Cell Biol, 2017. **19**(8): p. 996-1002.
8. Yu, F.X. and K.L. Guan, *The Hippo pathway: regulators and regulations.* Genes Dev, 2013. **27**(4): p. 355-71.
9. Jaffe, A.B. and A. Hall, *Rho GTPases: biochemistry and biology.* Annu Rev Cell Dev Biol, 2005. **21**: p. 247-69.
10. Mo, J.S., et al., *Cellular energy stress induces AMPK-mediated regulation of YAP and the Hippo pathway.* Nat Cell Biol, 2015. **17**(4): p. 500-10.

11. Garcia, M.A., W.J. Nelson, and N. Chavez, *Cell-Cell Junctions Organize Structural and Signaling Networks.* Cold Spring Harb Perspect Biol, 2018. **10**(4).

12. Irvine, K.D., *Integration of intercellular signaling through the Hippo pathway.* Semin Cell Dev Biol, 2012. **23**(7): p. 812-7.

13. Dupont, S., et al., *Role of YAP/TAZ in mechanotransduction.* Nature, 2011. **474**(7350): p. 179-83.

14. Zhao, B., et al., *Cell detachment activates the Hippo pathway via cytoskeleton reorganization to induce anoikis.* Genes Dev, 2012. **26**(1): p. 54-68.

15. Zanconato, F., et al., *YAP/TAZ as therapeutic targets in cancer.* Curr Opin Pharmacol, 2016. **29**: p. 26-33.

16. Steinhardt, A.A., et al., *Expression of Yes-associated protein in common solid tumors.* Hum Pathol, 2008. **39**(11): p. 1582-9.

17. Sun, Z., et al., *Prognostic Value of Yes-Associated Protein 1 (YAP1) in Various Cancers: A Meta-Analysis.* PLoS One, 2015. **10**(8): p. e0135119.

18. Calses, P.C., et al., *Hippo Pathway in Cancer: Aberrant Regulation and Therapeutic Opportunities.* Trends Cancer, 2019. **5**(5): p. 297-307.

19. Pan, D., *The hippo signaling pathway in development and cancer.* Dev Cell, 2010. **19**(4): p. 491-505.

20. Liu-Chittenden, Y., et al., *Genetic and pharmacological disruption of the TEAD-YAP complex suppresses the oncogenic activity of YAP.* Genes Dev, 2012. **26**(12): p. 1300-5.

21. Varelas, X., *The Hippo pathway effectors TAZ and YAP in development, homeostasis and disease.* Development, 2014. **141**(8): p. 1614-26.

22. Willey, C., et al., *Analysis of Nationwide Data to Determine the Incidence and Diagnosed Prevalence of Autosomal Dominant Polycystic Kidney Disease in the USA: 2013-2015.* Kidney Dis (Basel), 2019. **5**(2): p. 107-117.

23. Palsson, R., et al., *Characterization and cell distribution of polycystin, the product of autosomal dominant polycystic kidney disease gene 1.* Mol Med, 1996. **2**(6): p. 702-11.

24. Wilson, P.D., *Polycystic kidney disease: new understanding in the pathogenesis.* Int J Biochem Cell Biol, 2004. **36**(10): p. 1868-73.

25. Tian, Y., et al., *TAZ promotes PC2 degradation through a SCFbeta-Trcp E3 ligase complex.* Mol Cell Biol, 2007. **27**(18): p. 6383-95.

26. Patil, A., et al., *Childhood Polycystic Kidney Disease*, in *Polycystic Kidney Disease*, X. Li, Editor. 2015: Brisbane (AU).

27. Ma, S. and K.L. Guan, *Polycystic kidney disease: a Hippo connection.* Genes Dev, 2018. **32**(11-12): p. 737-739.

28. Takakura, A., et al., *Pkd1 inactivation induced in adulthood produces focal cystic disease.* J Am Soc Nephrol, 2008. **19**(12): p. 2351-63.

29. Ueno, T., et al., *Liver and kidney transplantation for polycystic liver and kidney-renal function and outcome.* Transplantation, 2006. **82**(4): p. 501-7.

30. Li, Z., et al., *Structural insights into the YAP and TEAD complex.* Genes Dev, 2010. **24**(3): p. 235-40.

31. Tian, W., et al., *Structural and functional analysis of the YAP-binding domain of human TEAD2.* Proc Natl Acad Sci U S A, 2010. **107**(16): p. 7293-8.

32. Hau, J.C., et al., *The TEAD4-YAP/TAZ protein-protein interaction: expected similarities and unexpected differences.* Chembiochem, 2013. **14**(10): p. 1218-25.

33. Santucci, M., et al., *The Hippo Pathway and YAP/TAZ-TEAD Protein-Protein Interaction as Targets for Regenerative Medicine and Cancer Treatment.* J Med Chem, 2015. **58**(12): p. 4857-73.

34. Mesrouze, Y., et al., *Adaptation of the bound intrinsically disordered protein YAP to mutations at the YAP:TEAD interface.* Protein Sci, 2018. **27**(10): p. 1810-1820.

35. Mesrouze, Y., et al., *Dissection of the interaction between the intrinsically disordered YAP protein and the transcription factor TEAD.* Elife, 2017. **6**.

36. Gibault, F., et al., *Toward the Discovery of a Novel Class of YAP(-)TEAD Interaction Inhibitors by Virtual Screening Approach Targeting YAP(-)TEAD Protein(-)Protein Interface.* Cancers (Basel), 2018. **10**(5).

37. Chan, P., et al., *Autopalmitoylation of TEAD proteins regulates transcriptional output of the Hippo pathway.* Nat Chem Biol, 2016. **12**(4): p. 282-9.

38. Holden, J.K. and C.N. Cunningham, *Targeting the Hippo Pathway and Cancer through the TEAD Family of Transcription Factors.* Cancers (Basel), 2018. **10**(3).

39. Noland, C.L., et al., *Palmitoylation of TEAD Transcription Factors Is Required for Their Stability and Function in Hippo Pathway Signaling.* Structure, 2016. **24**(1): p. 179-186.

40. Zhou, Z., et al., *Targeting Hippo pathway by specific interruption of YAP-TEAD interaction using cyclic YAP-like peptides.* The FASEB Journal, 2015. **29**(2): p. 724-732.

41. Marqus, S., E. Pirogova, and T.J. Piva, *Evaluation of the use of therapeutic peptides for cancer treatment.* J Biomed Sci, 2017. **24**(1): p. 21.

42. Bressler, N.M. and G. Treatment of Age-Related Macular Degeneration with Photodynamic Therapy Study, *Photodynamic therapy of subfoveal choroidal neovascularization in age-related macular degeneration with verteporfin: two-year results of 2 randomized clinical trials-tap report 2.* Arch Ophthalmol, 2001. **119**(2): p. 198-207.

43. Chen, Q., et al., *A temporal requirement for Hippo signaling in mammary gland differentiation, growth, and tumorigenesis.* Genes Dev, 2014. **28**(5): p. 432-7.

44. Dong, L., et al., *Verteporfin inhibits YAP-induced bladder cancer cell growth and invasion via Hippo signaling pathway.* Int J Med Sci, 2018. **15**(6): p. 645-652.

45. Giraud, J., et al., *Verteporfin targeting YAP1/TAZ-TEAD transcriptional activity inhibits the tumorigenic properties of gastric cancer stem cells.* Int J Cancer, 2020. **146**(8): p. 2255-2267.

46. Feng, J., et al., *Verteporfin, a suppressor of YAP-TEAD complex, presents promising antitumor properties on ovarian cancer.* Onco Targets Ther, 2016. **9**: p. 5371-81.

47. Dasari, V.R., et al., *Verteporfin exhibits YAP-independent anti-proliferative and cytotoxic effects in endometrial cancer cells.* Oncotarget, 2017. **8**(17): p. 28628-28640.

48. Donohue, E., et al., *Induction of Covalently Crosslinked p62 Oligomers with Reduced Binding to Polyubiquitinated Proteins by the Autophagy Inhibitor Verteporfin.* PLoS One, 2014. **9**(12): p. e114964.

49. Bum-Erdene, K., et al., *Small-Molecule Covalent Modification of Conserved Cysteine Leads to Allosteric Inhibition of the TEADYap Protein-Protein Interaction.* Cell Chem Biol, 2019. **26**(3): p. 378-389 e13.

50. Feng, X., et al., *IL1R1 is required for celastrol's leptin-sensitization and antiobesity effects.* Nat Med, 2019. **25**(4): p. 575-582.

51. Allen, G.I., et al., *Crowdsourced estimation of cognitive decline and resilience in Alzheimer's disease.* Alzheimers Dement, 2016. **12**(6): p. 645-53.

52. Liu, J., et al., *Treatment of obesity with celastrol.* Cell, 2015. **161**(5): p. 999-1011.

53. Jameson D.M., Seifried S.E. *Quantification of protein-protein interactions using fluorescence polarization*. Methods. 1999;19(2):222-233.

54. Wallach, I., et al., *AtomNet: A Deep Convolutional Nerual Network for Bioactivity Prediction in Structure-based Drug Discovery*. 2015.

CURRICULUM VITAE

ABIGAIL FISK THOMPSON

EDUCATION

Indiana University — Indianapolis, IN

Master of Science, Biochemistry and Molecular Biology — **September 2020**

Indiana University — Bloomington, IN

Bachelor of Science, Biochemistry — **May 2019**

High Distinction

Certificate in Human Biology

HONORS AND AWARDS

Phi Beta Kappa Inductee	December 2019
Lilly Endowment Scholarship	2015 – 2019
Indiana University Provost Scholarship	2015 – 2019